geologica acta

Citation: Oskay, R.G., 2025. Coal properties of Carboniferous Kurtköy coals (Zonguldak, NW Türkiye): Emphasis on rank, provenance of minerals and hydrocarbon generation potential. Geologica Acta, 23.16, 1-31. DOI: 10.1344/Geologica2025.23.16

Online ISSN: 1696-5728

Coal properties of Carboniferous Kurtköy coals (Zonguldak, NW Türkiye): Emphasis on rank, provenance of minerals and hydrocarbon generation potential

Rıza Görkem Oskay[1]

[1]**Başkent OSB Technical Sciences Vocational School, Hacettepe University**

Başkent OSB No.20 06909 Malıköy Sincan/Ankara, Türkiye. E-mail: rizagorkemoskay@hacettepe.edu.tr

ABSTRACT

Late Carboniferous coal seams in the Zonguldak Basin (NW Türkiye) underwent several tectonic movements after the Late Permian; hence, these seams exhibit rank variations. This study presents initial insights into coal rank, mineralogical compositions, and hydrocarbon generation potential of Serpukhovian-Bashkirian coals within the Alacaağzı Formation from the south-easternmost part of the Basin. The examined seams are of bituminous C rank, and T_{max} (442–445°C) and HI (221–288mg HC/g TOC) values indicate that they are at the set of oil generation. However, the low PI (0.01–0.02), BI (0.03–0.06), and QI (2.2–2.9) values and the possible presence of preserved cytoplasm spore-filling within the sporinite grains may indicate that the studied coals have only gas-generation potential. The results also show that the studied coals display relatively lower random vitrinite reflectance (%Rr 0.75–0.82%) and calculated Tpeak values (113–123ºC) using %Rr and micro-Raman spectra than their counterparts in the northern parts of the Basin (%Rr 1.18–1.52% and 173–206ºC). This difference seems to be related to the shallower burial depths of the studied coals or to the fact that they experienced relatively lower maximum attained temperatures than the northern parts of the Basin. Furthermore, the coal petrography and SEM-EDS data also suggest that the post-coalification tectonic deformation in the study area created space for circulating Ca- and Si-rich solutions within the coal seams and controlled epigenetic mineralization. Nevertheless, the redox conditions and clastic influx into the palaeomires also controlled syngenetic mineral formations, similar to the other parts of the Basin.

KEYWORDS | **Carboniferous. Coal petrography. Mineralogy. Zonguldak Basin. Rock-Eval pyrolysis.**

INTRODUCTION

Tectonic deformation during post-coalification could affect the rank, thermal maturity, porosity, and mineralogical composition of coal seams (Frodsham and Gayer, 1999; Liu and Jiang, 2019; Li *et al.*, 2011; Ren *et al.*, 2022; Wang *et al.*, 2021). Such impacts could also create severe problems for underground coal mining activities (Cao *et al.*, 2003; Li *et al.*, 2023). Therefore, coal seams close to regional tectonic zone should be investigated by the means of coal petrography, mineralogy, and porosity to eliminate any future problems. Coal seams in the Zonguldak Basin (Fig. 1A, B) could be a good example for such conditions since several faults and folds have been observed within coal production areas (Okay and Tüysüz, 1999; Okay and Nikishin, 2015; Okay *et al.*, 1994), and several gas outbursts have occurred in the past (Fisne and Esen, 2014). The Zonguldak Basin (NW Türkiye) hosts the oldest coal production, which has been started at 1848, area in Türkiye and almost all Turkish bituminous coal resources (ca 1.5Gt). It is also located in the eastern parts of the Istanbul Zone, which was positioned in the southern margin of Laurasia during

the Late Palaeozoic (Karayiğit *et al.*, 1998, 2018a; Opluštil *et al.*, 2018; Yalçin *et al.*, 2002). The basin experienced several orogenic movements from the Late Carboniferous to the Neogene (Okay and Nikishin, 2015; Okay *et al.*, 1994; Tüysüz, 1999; Yilmaz *et al.*, 1997). This part of Laurasia is considered as a passive margin and collided with Pontides during the Variscan (Hercynian) orogeny. Therefore, the basin was uplifted and experienced erosional events during the Permian. The Cimmeride orogeny as the second orogenic movement affected the basin, and the subduction of the Pontides under Laurasia continued between the Late Triassic and Early Cretaceous. During this period, carbonate sedimentation was more common in the basin; therefore, the Cimmeride orogeny could not be identified in the Zonguldak Basin. With the start of the elimination of the Neotethys from the Late Cretaceous, a collision between the Pontide arc and the Anatolid-Tauride platform took place. This collision has continued since the Middle Eocene in the Zonguldak Basin and its vicinity. Consequently, several thrust fault zones and folds in the Zonguldak Basin were formed, and the coal-bearing Carboniferous sequences in the basin were deformed, thrust over, and exposed to erosion. Hence, rank variations have been observed in Late Carboniferous coal seams within the Zonguldak Basin (Karayiğit, 1992; Karayiğit *et al.*, 1998, 2018a; Yalçin *et al.*, 2023).

Previous coal petrography, mineralogy and Rock-Eval pyrolysis studies mostly focused on coal seams in the Kozlu (Langsettian) and Karadon (Duckmantian–Asturian) formations (fms.) (Karayigit, 1992, 2003, 2001; Ünal-Kartal and Karadirek, 2024; Hoşgörmez *et al.*, 2002; Kara-Gülbay *et al.*, 2019; Karayiğit *et al.*, 2018b; Yalçin *et al.*, 2002, 2023), whereas limited attempts have been made for coal seams within the Serpukhovian–Bashkirian Alacaağzı Fm. in the northern parts of the Zonguldak Basin (Karayiğit *et al.*, 1998, 2018a). The results of previous studies indicate that the coal seams within the Alacaağzı Fm. in the Zonguldak coalfields generally display higher random vitrinite reflectance (%Rr) values (1.18–1.52%) than other coal seams in the Kozlu (0.66–1.49%) and Karadon (0.55–1.01%) fms. in the Zonguldak and Amasra coalfields, except for the thermally affected coal seams in the central parts of the Zonguldak coalfields, which are bituminous B–C (medium B–C) coal (Karayiğit, 1992; Karayiğit *et al.*, 2018b; Yalçin *et al.*, 2002, 2023). Moreover, coal seams within the Alacaağzı Fm. in the Kurtköy coalfield, which is located in the South-easternmost part of the Zonguldak coalfields (Fig. 1B), and to date, petrographical, mineralogical, and Rock-Eval pyrolysis features of these seams have not been studied in detail. The goal of this research is to identify the factors that influence coal quality, mineralogical compositions, and hydrocarbon generation potential of Serpukhovian–Bashkirian coals in the Kurtköy coalfield (South easternmost of the Zonguldak Basin).

GEOLOGICAL SETTING

The Zonguldak Basin is located in conjunction with the Istanbul Zone and western Pontides (Fig. 1A–C), and it hosts Palaeozoic metamorphic and sedimentary rocks, Mesozoic clastic rocks and marine carbonates, and Cenozoic volcanic and sedimentary rocks (Okay and Nikishin, 2015; Gorur *et al.*, 1993; Tüysüz *et al.*, 2016; Yalçin *et al.*, 2002; Yilmaz *et al.*, 1997). Mesozoic and Cenozoic formations in the basin are also called "post-Carboniferous cover formations" (Karayiğit *et al.*, 2018a; Yalçin *et al.*, 2002). Paleozoic sequences in the basin start with metasediments from the Silurian Göktepe and Hamzafakılı fms., and the Late Devonian–Early Carboniferous (Tournaisian–Visean) Yılanlı Fm. (Fig. 1C) (Kerey, 1984; Kerey *et al.*, 1986; Yalçin *et al.*, 2002; Yilmaz *et al.*, 1997). The coal-bearing Serpukhovian–Bashkirian Alacaağzı Fm. commences to deposit a transition between shallow marine and deltaic conditions, and the thickness of the formation (up to 1100m) is variable in the basin (Okan and Hoşgör, 2007; Kerey *et al.*, 1986; Opluštil *et al.*, 2018). The formation is primarily composed of alternating sandstone, siltstone, claystone, and coal seams (Fig. 1C) (Karayigit *et al.*, 1998, 2018a; Kerey *et al.*, 1986; Yalçin *et al.*, 2002). Previous sedimentological and paleontological studies have suggested that coal-bearing sequences in the Alacaağzı Fm. were deposited in fluvial and deltaic environments during the Serpukhovian and Bashkirian periods (Ağralı, 1970; Akgün and Akyol, 1992; Kerey *et al.*, 1986).

Despite some evidence suggested erosional periods in the Bashkirian–Langsettian Basin being reported from the Zonguldak Basin (Kerey, 1984; Zijlstra, 1952; Opluštil *et al.*, 2018), the Kozlu Fm., rests generally upon conformably the Alacağzı Fm. (Fig. 1C). The formation is mainly composed of alternations of conglomerate, sandstone, siltstone, claystone, and coal seams (Fig. 1C). The precursor peats of the coal seams within Kozlu Fm. accumulated in deltaic and lacustrine environments during the Langsettian (Akyol, 1974; Kerey, 1984; Akgün and Akyol, 1992; Cleal and van Waveren, 2012; Karayiğit *et al.*, 2018a; Opluštil *et al.*, 2018). Karadon Fm. conformably overlays the Kozlu Fm. and consists of conglomerate, sandstone, siltstone, claystone, and coal seams alternations, which were deposited under deltaic and lacustrine conditions during the Duckmantian–Asturian (Akyol, 1974; Cleal and van Waveren, 2012; Karayiğit *et al.*, 2018a; Kerey *et al.*, 1986; Opluštil *et al.*, 2018). In the Kozlu and Karadon fms. in the Zonguldak and Amasra coalfields, tonstein/altered tuff layers (locally known as Schieferton), which are mainly composed of kaolinite, could be indicators of synchronous volcanic activity during the Late Carboniferous in the vicinity of the Zonguldak Basin (Burger *et al.*, 2000; Karayiğit *et al.*, 2018a, 2022). The Zonguldak Basin experienced erosional events during the Permian, similar

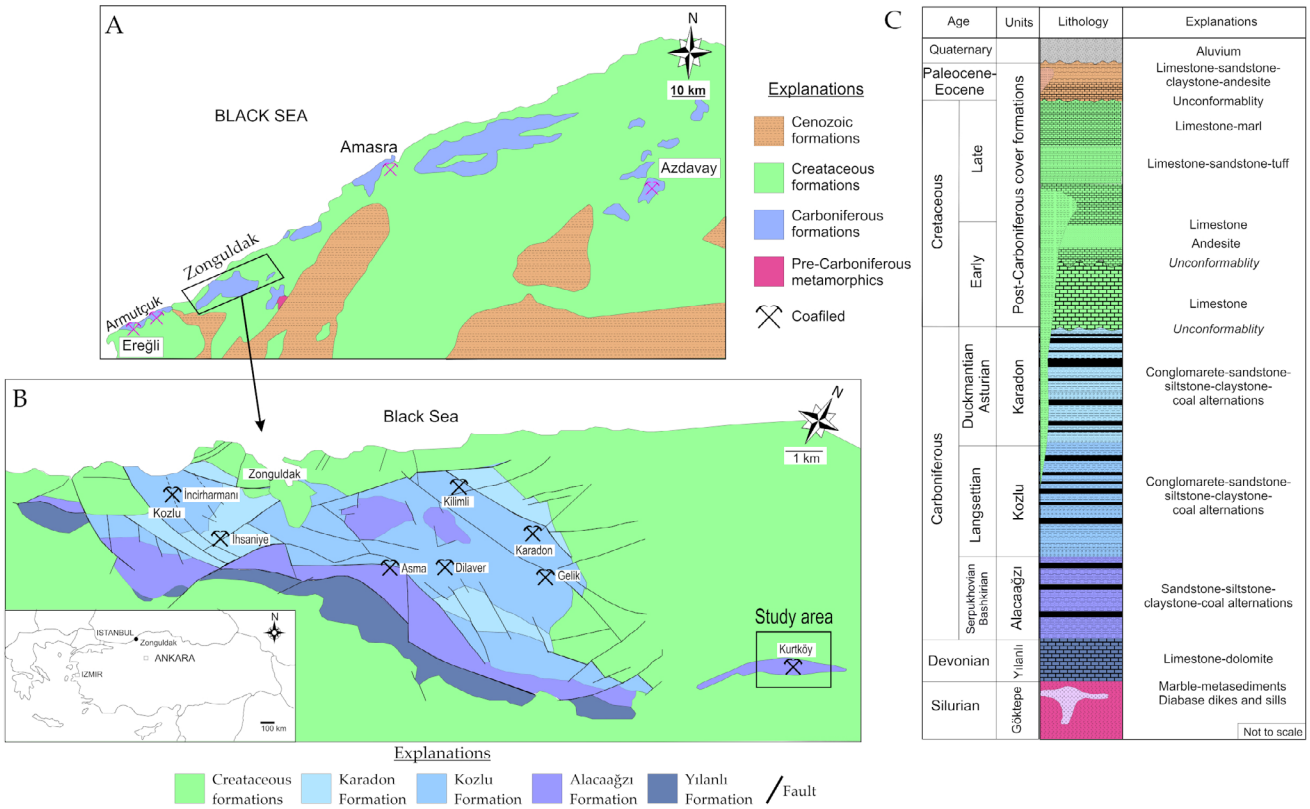

FIGURE 1. A, B) Geologic map of the Zonguldak Basin (modified and simplified from Karayiğit *et al.* (2018a) and Opluštil *et al.*, 2018) and stratigraphic column of the Zonguldak Basin (modified fromKarayiğit *et al.* (2018b).

to other Carboniferous basins in SE Europe, because of the Hercynian (Variscan) orogeny (Karayiğit *et al.*, 2018a; Yalçin *et al.*, 2002). Therefore, the Cretaceous and Paleocene–Eocene fms. in the basin unconformable overlay the Carboniferous formations (Fig. 1C), and these post-Carboniferous formations are mostly composed of Cretaceous clastic and marine carbonates in the Zonguldak coalfields (Fig. 1B). Cretaceous dikes and sills have also been reported in the coalfields in the Zonguldak area, and thermally affected coals have been reported close to these dykes (Karayiğit, 1992). The collision of the Sakarya and İstanbul zones during the Eocene and Alpine orogeny caused the formation of several faults and folds within the coalfields in the Zonguldak Basin (Fig. 1A), as well as additional deformations of Carboniferous and post-Carboniferous cover formations in the basin (Okay and Tüysüz, 1999; Okay and Nikishin, 2015; Okay *et al.*, 1994; Yilmaz *et al.*, 1997).

MATERIALS AND METHODS

In this study, twelve fresh coal samples (SO-4 to SO-15) from working coal seams at an underground mine and three coal samples (SO-1 to SO-3) from outcrops proximal to the studied underground mine in the Kurtköy coalfield were examined (Table 1). All the samples were obtained utilizing the channel sampling method. For macroscopic descriptions of samples, the macrolithotype classification of International Coal and Organic Petrography (ICCP) for bituminous coals was applied according to the protocols of ICCP (ICCP, 1993). The standard proximate, ultimate, and calorific analyses of samples were performed at Hacettepe University using related American Society for Testing and Materials (ASTM) standards (ASTM D3174, 2018; ASTM 4239, 2018; ASTM D5865, 2019; ASTM D3175, 2020; ASTM D5373, 2021; ASTM D3302, 2022). Polished blocks were prepared in accordance with ASTM D2797/D2797M (2021) standard and were examined under a Leica DM4000M microscope. The maceral classifications were conducted following the ICCP System 1994 (ICCP, 1998, 2001; Pickel *et al.*, 2017), and random vitrinite reflectance (%Rr) was measured on collotellinite following the ISO 7404–5 (2009) standard.

The mineralogical compositions of raw coal samples were determined using X-Ray powder Diffraction (XRD) traces, and mineralogical compositions were identified using Topas 3 software following Oskay *et al.* (2016). Additionally, FT-IR analyses were only conducted on

TABLE 1. The results of proximate, ultimate and calorific analyses of studied coal samples (VM: Volatile Matter, FC: Fixed Carbon, GCV: Gross Calorific Values, ad: air-dry basis, d: dry basis)

Sample ID	UTM Coordinates (m) y (east)	x (north)	z (elevation)	Moisture	Ash	VM	FC	GCV (MJ/kg, ad)	C	H	N	S	O*
				(wt%, ad)					(wt%, d)				
SO-1	4589999	409825	+326	9.8	29.2	29.9	31.1	13.8	47.2	3.1	0.7	0.2	16.4
SO-2	4590095	409825	+326	10.8	25.1	33.1	30.9	15.8	51.9	3.5	0.9	0.6	14.9
SO-3	4590414	410198	+376	1.7	7.9	29.8	60.5	31.5	82.0	4.4	1.1	0.8	3.7
SO-4	4592660	413395	+382	1.6	16.1	32.4	50.0	28.7	72.2	4.5	1.4	1.5	4.0
SO-5	4592640	413387	+412	1.6	7.4	34.6	56.4	31.9	80.2	4.9	1.5	1.8	4.1
SO-6	4592622	413384	+422	1.6	15.4	33.1	49.9	28.9	73.2	4.6	1.4	1.3	3.9
SO-7	4592682	413454	+386	1.6	20.3	31.5	46.6	27.2	69.1	4.3	1.3	1.3	3.3
SO-8	4592688	413463	+379	1.5	10.9	34.5	53.1	30.7	77.5	4.8	1.4	0.9	4.3
SO-9	4592599	413201	+362	1.3	14.3	34.4	50.0	28.5	74.6	4.7	1.4	0.8	4.1
SO-10	4593008	413361	+294	1.3	6.7	36.6	55.4	32.4	79.6	4.6	1.5	0.6	7.0
SO-11	4593052	413919	+294	1.3	7.4	36.8	54.5	32.0	81.3	4.8	1.5	0.8	4.0
SO-12	4593086	413935	+279	1.2	12.4	35.8	50.7	28.3	79.9	4.8	1.6	0.8	0.4
SO-13	4593196	413999	+299	1.4	6.9	36.5	55.3	28.9	74.9	4.3	1.4	0.8	11.6
SO-14	4593202	413980	+296	1.6	6.3	35.7	56.5	31.3	81.3	5.1	1.6	1.1	4.5
SO-15	4592894	413696	+306	1.2	8.9	35.2	54.7	31.5	82.2	5.0	1.5	0.8	1.4

*oxygen content is calculated from other analytical data [O = 100 − (C + H + S + N + ash)]

selected four samples (SO-2, -7, -9, and -14) according to XRD analyses, and measurements were made using grounded raw samples below 250μm. The selected five samples (SO-2, -4, -7, -12 and -15) based on mineralogical compositions and coal petrography observations were examined under Scanning Electron Microscopes equipped with Energy-Dispersive X-ray Spectroscopy (SEM-EDS) to investigate cleat/fracture mineral infillings and to identify accessory mineral phases. The polished blocks of samples have been coated with carbon for SEM-EDS analysis. The XRD, FTIR and SEM analyses of samples were conducted at the General Directorate of Mineral Research and Exploration (MTA). The Raman spectroscopic experiments were performed on three selected polished blocs (SO-7, -9, and -14), which were selected to their maceral compositions, prepared for coal petrography using a HORIBA Jobin Yvon LabRAM HR spectrometer according to methodology reported by Guedes *et al.* (2010) and Li *et al.* (2020) at the University of Patras. Raman spectra were acquired using the 532nm excitation line with an acquisition time of 5s to reduce noise. Raman spectra were measured with a density filter to avoid thermal decomposition of samples by the laser. The ×50 objective lens (N.A= 0.50) of an Olympus optical microscope was used to focus the laser beam on the sample and also to collect the scattered radiation. Extended scans from 1000 to 1800cm^{-1} for the first-order Raman spectrum were performed on each sample. The peak-fitting process was achieved using Lab Spec Software following the methods described in Matlala *et al.* (2024).

To assess the hydrocarbon generation potential of the samples, Rock-Eval pyrolysis analysis of twelve samples (SO-4 to SO-15) was only performed using Rock-Eval 6 equipment at Turkish Petroleum Co. (TPAO) following the methodologies of Espitalié *et al.* (1977) and Lafargue *et al.* (1998). The accuracy of the analysis was verified using IFP 160,000 standard material. The following parameters were calculated using Rock-Eval analysis results: T_{max}, Total Organic Carbon (TOC), Oxygen Index (OI), Hydrogen Index (HI), Pyrolyzed Carbon (PC), Residual Carbon (RC) and Mineral Carbon (MINC). Additionally, effective HI and HI_{max} values were calculated according to Petersen (2006) and Sykes and Snowdon (2002) to provide a more accurate estimation of hydrocarbon generation compared to traditional parameters.

RESULTS

Standard coal quality

Comparatively higher ash yields and lower gross calorific values were observed in the coal samples (SO-1 and -2) obtained from the outcrops (Table 1). In contrast, the working seam samples (SO-4 to -15) were characterized by low to moderate ash yields and high total C and gross calorific values (Table 1). The difference in ash yield between the outcrop and the working seams seems to be related to the surface weathering impact of outcrop samples; in turn, their total C and gross calorific values are slightly lower than those of the working seam samples (Table 1). This difference is evident in the outcrop sample SO-3 since epigenetic mineralization (pyrite and Fe-oxide cleat/fracture infillings) is less common than other outcrop samples. The volatile matter contents of all samples were generally high, and as can be seen in Section 4.3, this seems

to be controlled by the presence of carbonate minerals in the samples. Similar to the total C content, outcrop samples generally have relatively lower total S contents than the working seam samples (Table 1). Surface weathering might have caused the oxidation of sulphide minerals (such as pyrite) in the outcrop samples; thus, leaching sulfate ions to solution from coal seams might have caused a reduction in total S contents of these samples. In comparison with the coal seams within the Alacaağzı Fm. in the Northwesternmost part of the Zonguldak coalfields, the studied samples displayed relatively lower ash yields and higher total C contents and gross calorific values (Karayigit *et al.*, 1998, 2018a).

Coal petrography and vitrinite reflectance

Vitrinite (61.0–87.4 vol.%. on mineral-matter free basis [mmf]) is the dominant maceral group in the samples, and the contents of inertinite (6.5–30.8 vol.%. on mmf) and liptinite (3.3–11.8 vol.%. on mmf) show a wide range (Table 2). Telovitrinite is the most common maceral sub-group in the working coal seams samples, while detrovitrinite is another common vitrinite subgroup maceral in the all studied samples (Table 2). In addition, gelovitrinite subgroup macerals are rarely observed in the samples. Tellinite general displays very low proportions in telovitrinite subgroup (Fig. 2A), while collotelinite is the predominant maceral in this group ((Figs. 2B–I; 3A–E; 4A). In the working seam samples, detrovitrinite subgroup is predominated by collodetrinite, and inertinite and liptinite group macerals are embedded within the humic matrix of collodetrinite (Fig. 2 C–E, G–I). In contrast with working coal seams samples, vitrodetrinite proportions are generally significantly high in out-crop samples (Table 2) and mostly associated with clay mineral matrix (Fig. 4A). Gelinite is the only identified gelovitrinite subgroup maceral in the working coal samples (Fig. 2H). In addition, brecciated macerals are observed from working coal seams samples (Fig. 3B–D), while limited oxidation rims and especially desiccation cracks in vitrinites are observed from outcrop samples, as expected.

In outcrop and working coal seam samples, the inertinite group maceral is mainly represented by fusinite, inertodetrinite, and micrinite. Fusinite (Figs. 2C, F; 3A) and inertodetrinite (Figs. 2E, G–I; 3B; 4A, E) particles are commonly found within the humic matrix of collodetrinite or associated with clay minerals. Additionally, individual fusinite and semifusinite have been identified in the samples. Micrinite is observed around inertinite and liptinite macerals within collodetrinitie matrix (Fig. 3C). In a few samples (SO-1, -7, -11 and-13), secretinite and macrinite are also detected. Sporinite and liptodetrinite are the common liptinite macerals, while cutinite and resinite are rarely identified in the studied samples. Sporinite is mostly related to microspores and macrospores (Figs. 2C–E, G–I; 3A–F; 4E). Latter ones in some cases could also contain preserved cytoplasm spore-filling (Fig. 3A, B), which is not so common for the Carboniferous coal seams in the Zonguldak Basin. Their presence could be attributed to a lower degree of coalification since such spore-fillings can easily devolatilize during early stages of coalification processes (Hower and Eble, 2022; Stout and Spackman, 1987; Hower *et al.*, 2022). In the northern parts the Zonguldak Basin, liptinite macerals in the Serpukhovian–Bashkirian coal seams appear darker under white-incident light and give off a brighter orange fluorescence under UV-blue light (Karayiğit *et al.*, 2018a). In contrast, liptinite macerals in the studied samples show darker colours under white-incident light and brighter orange fluorescence colour under UV-blue light. This could be due to their relatively lower level of coalification compared to the other Serpukhovian–

TABLE 2. The maceral composition and random vitrinite reflectance of studied samples (T: Telinite, Ct: Collotelinite, TV: Telovitrinite, Vd: Vitrodetrinite, Cd: Collodetrinite, DV: Detrovitrinite, Gl: Gelinite, GV: Gelovitrinite, V: Vitrinite, I: Inertinite, L: Liptinite, MM: Mineral-Matter, Stdv: Standard deviation)

Sample ID	Maceral (vol.%, mineral-matter-free)											MM (vol.%, whole basis)	%Rr±Stdv
	T	Ct	TV	Vd	Cd	DV	Gl	GV	V	I	L		
SO-1	2.4	33.3	35.7	21.6	14.5	36.1			71.8	24.4	3.8	9.4	0.82±0.03
SO-2	0.2	43.6	43.8	15.1	28.5	43.6			87.4	6.5	6.1	12.0	0.82±0.03
SO-3	5.1	42.4	47.5	4.0	26.4	30.4			77.9	13.4	8.7	9.3	0.82±0.03
SO-4	1.9	55.6	57.5	7.7	10.8	18.5			76.0	13.4	10.6	7.3	0.77±0.02
SO-5	1.6	61.8	63.4	3.1	7.9	11.0			74.4	17.9	7.7	2.4	0.77±0.02
SO-6	1.6	54.5	56.1	7.5	12.4	19.9	0.4	0.4	76.4	15.4	8.2	7.0	0.77±0.02
SO-7	0.6	47.2	47.8	13.9	20.4	34.3			82.1	12.5	5.4	12.8	0.76±0.02
SO-8	3.1	51.9	55.0	3.1	20.4	23.5	1.2	1.2	79.7	11.9	8.4	1.9	0.77±0.02
SO-9	1.4	43.6	45.0	4.5	20.4	24.9	1.0	1.0	70.9	17.3	11.8	9.1	0.77±0.02
SO-10	1.5	38.5	40.0	1.4	19.5	20.9	0.6	0.6	61.5	30.8	7.7	1.7	0.76±0.02
SO-11	3.1	37.8	40.9	3.4	24.2	27.6	0.8	0.8	69.3	23.3	7.4	0.8	0.75±0.03
SO-12	2.5	48.2	50.7	3.5	21.2	24.7	0.6	0.6	76.0	20.7	3.3	0.4	0.77±0.02
SO-13	1.0	37.5	38.5	3.1	19.2	22.3	0.2	0.2	61.0	28.5	10.5	2.3	0.77±0.02
SO-14	0.5	53.9	54.4	7.7	22.2	29.9			84.3	9.2	6.5	1.6	0.78±0.02
SO-15	1.7	46.6	48.3	3.5	22.0	25.5			73.8	15.4	10.8	1.8	0.77±0.03

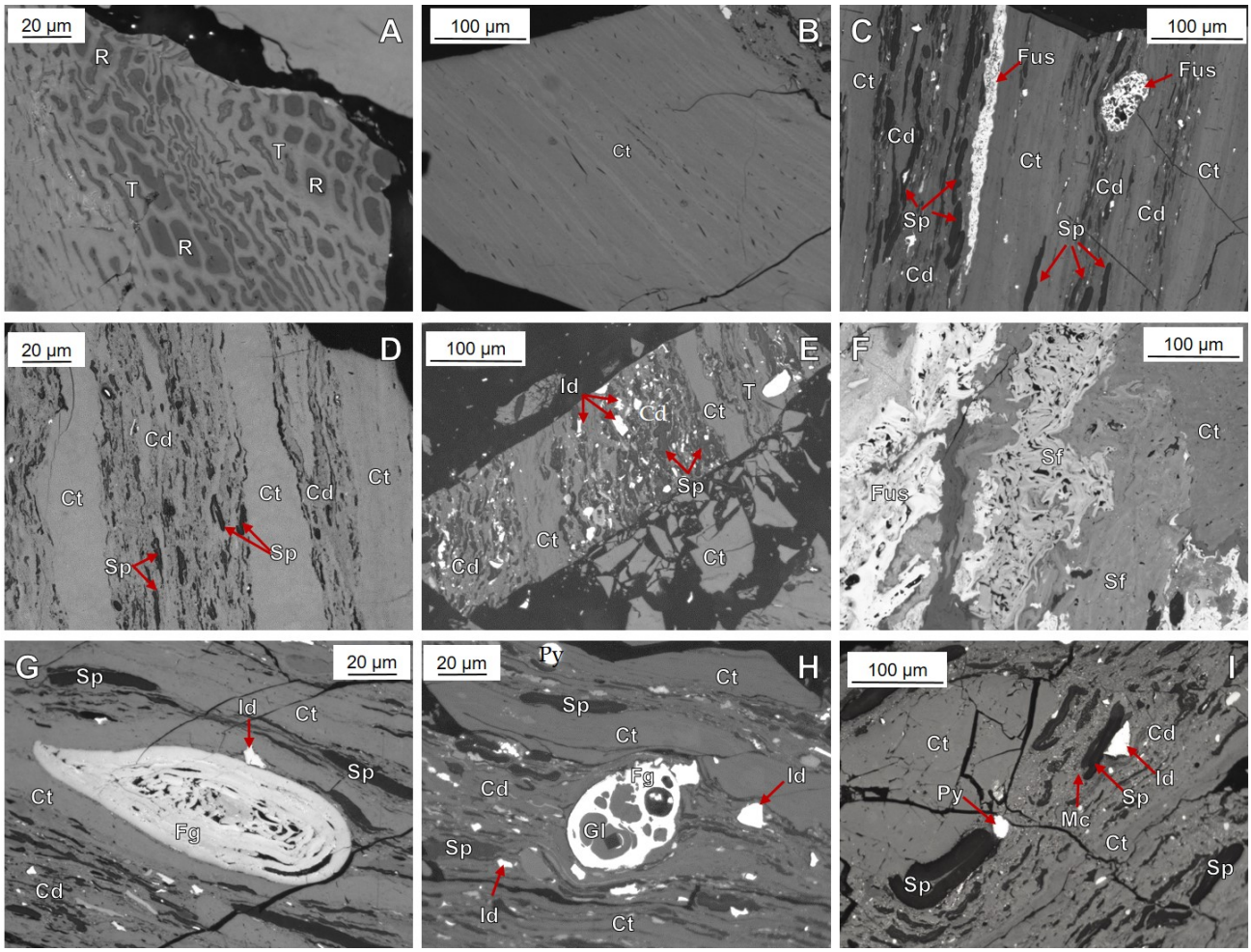

FIGURE 2. Selected photomicrographs of the studied samples. All photomicrographs are taken under incident white light, oil immersion, 500× total magnification. Telinite (T), Collotelinite (Ct), Collodetrinite (Cd), Resinite (R), Sporinite (Sp), Fusinite (Fus), Semifusinite (Sf), Inertodetrinite (Id), Gl) lGelinite, Micrinite (Mc), Funginite (Fg), Pyrite (Py). Photomicrograph A from SO-3, B and I from SO-15, C from SO-11, D, E and H from SO-8, G from SO-7.

Bashkirian coal seams in the basin. The mineral matter identified using white-incident light includes pyrite, clay minerals, and carbonate minerals. Clay minerals are mostly found as part of aggregates associated with vitrodetrinite, sporinite and inertodetrinite, along with other mineral matters (Fig. 4A). Carbonate minerals are only detected within cleat/fractures of vitrinite macerals, particularly brecciated ones (Fig. 4B–D). Pyrite is commonly observed as framboidal grains (Fig. 3E) and occasional cleat/fracture infillings (Fig. 4F).

The %Rr values of the outcrop samples are around 0.82%±0.02, while those of the working coal seams samples range between 0.75–0.78%±0.02 (Table 2). The %Rr values of working coal seams are slightly lower than the reported %Rr values of coal seams in the Alacaağzı Fm. in the northern parts of the Zonguldak Basin, and close reported %Rr values from Alacaağzı Fm. in the North-easternmost of the basin (Amasra coalfield), Kozlu and Karadon fms. (Karayiğit, 1992; Karayigit *et al.*, 1998, 2018a, b; Yalçin *et al.*, 2002, 2023).

Mineralogical composition

Clay minerals (kaolinite, chlorite, and illite/mica), calcite, and pyrite were detected in the raw coal samples by XRD (Table 3). Clay minerals are typically recognized as dominant phases in all investigated samples, whereas calcite is abundant-to-dominant phase only in the working seam samples (Table 3). Quartz is frequently found in working seam samples as a minor-to-abundant phase. Pyrite was absent in the XRD patterns in the outcrop samples; however, it was generally detected as a minor phase from the working coal seams (Table 3). Dolomite was also found as a minor phase in one sample (SO-15) (Table 3). In addition, the following minerals are identified as accessory phases: ankerite/Fe-dolomite, barite, biotite, chalcopyrite, Fe-oxides, feldspars, REE-

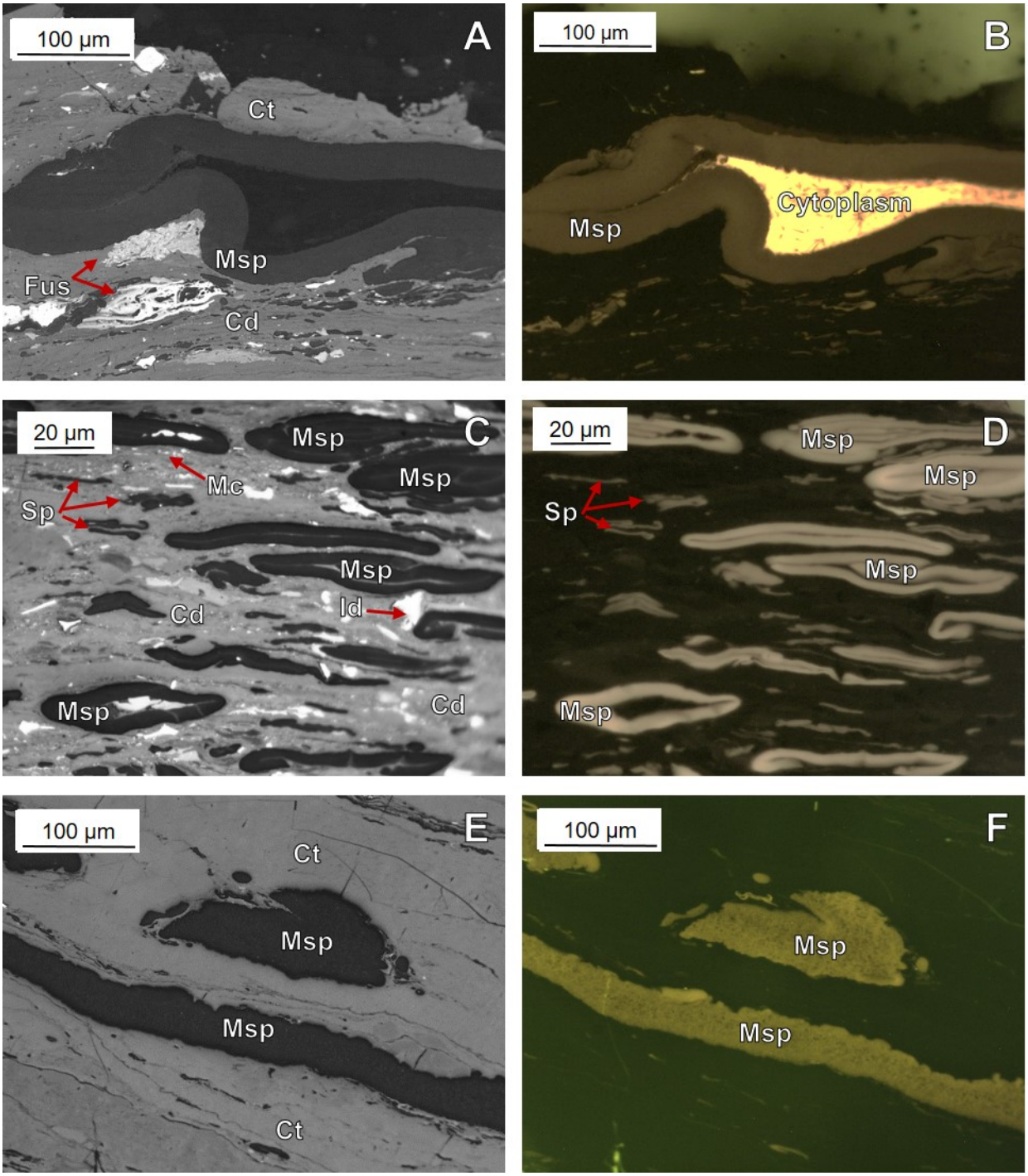

FIGURE 3. Selected photomicrographs of the studied samples. All photomicrographs are taken under incident white light (A, C and E) and blue-light excitation (B, D and F), oil immersion, 500× total magnification. Collotelinite (Ct), Collodetrinite (Cd), Sporinite (Sp), Megaspore (Msp), Micrinite (Mc), Fusinite (Fus) and Inertodetrinite (Id), Photomicrograph A from SO-3, B and I from SO-15, C from SO-11, D, E and H from SO-8, G from SO-7.

bearing goyazite, siderite, Ti-oxides, and zircon (Table 3). The identified minerals in the studied samples are similar to other reported mineralogical compositions of the Serpukhovian–Bashkirian coal seams in the Alacaağzı Fm. from Zonguldak coalfields (Karayigit, 2001, 2003; Karayiğit *et al.*, 2018a, 2018b).

FT-IR Analysis

The FT-IR spectra of the samples are mostly in agreement with the XRD data, and the FT-IR spectra of the analysed samples S0-2, -7, -9 and -14 are reported in Figure 5. The bands at approximately wavenumbers

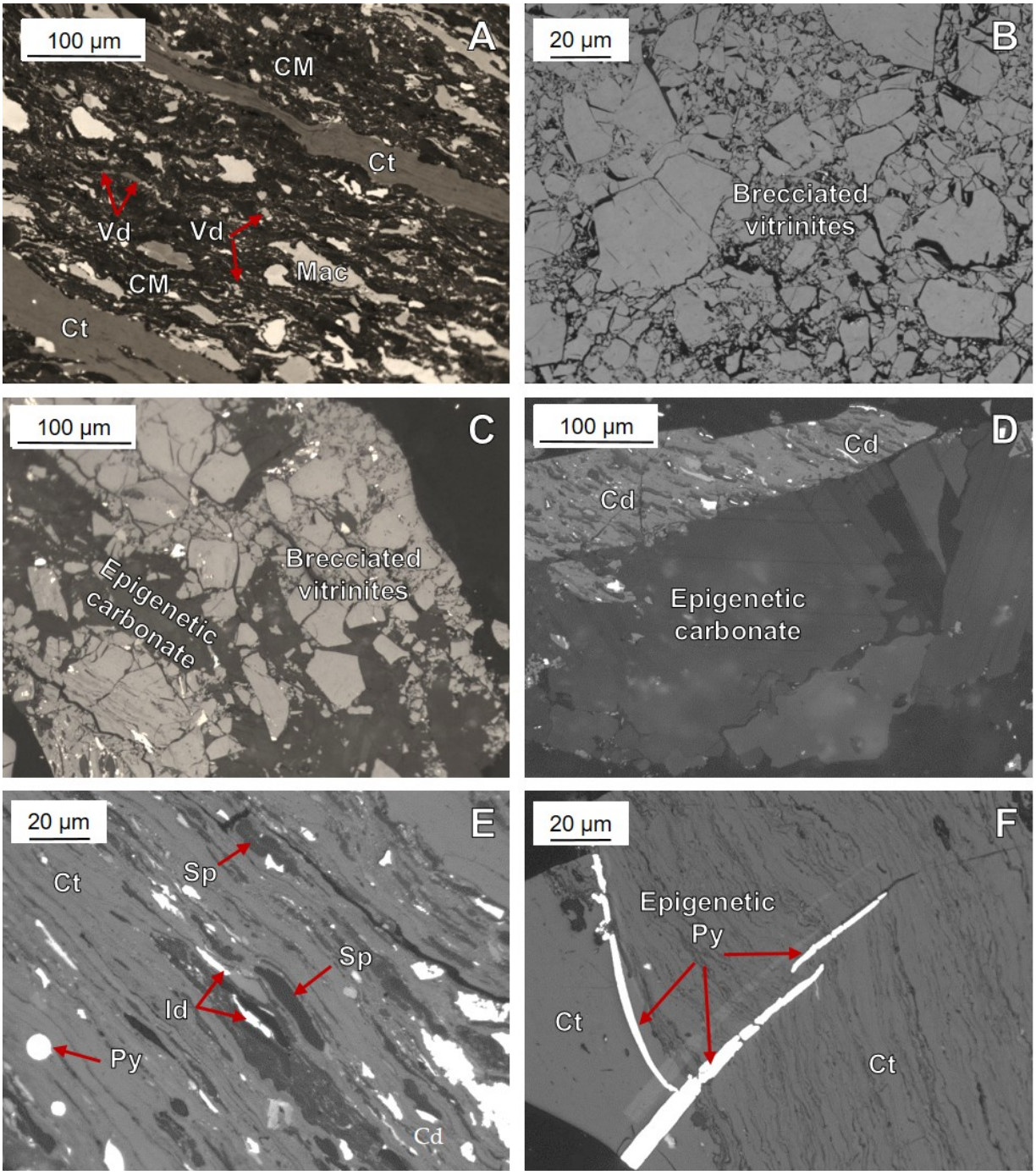

FIGURE 4. Selected photomicrographs of the studied samples. All photomicrographs are taken under incident white light, oil immersion, 500× total magnification. Collotelinite (Ct), Collodetrinite (Cd), Vitrodetrinite (Vd), Sporinite (Sp), Inertodetrinite (Id), Macrinite (Mac), Clay Mineral (CM) and Pyrite (Py). Photomicrograph A-B from SO-13, C-D from SO-11, E-F from SO-8.

3400, 1030, and 530cm^{-1} are related to clay minerals (Madejová, 2003; Tironi *et al.*, 2012). Nevertheless, the intense and wide band at 3400cm^{-1} could be an indicator of the OH-stretching vibration (Madejová, 2003; Jiang *et al.*, 2021), and the lack of characteristic bands at 3700, 3670, 3650, and 3620cm^{-1} for kaolinite could imply that kaolinite in the samples could be disordered (Tironi *et al.*, 2012). Quartz/silica in the samples could be attributed to the band around 470cm^{-1}, and this peak along with 1100cm^{-1} are not distinct in samples SO-9 and -14 (Fig. 5). This could not imply a lack of quartz/silica in the samples; instead, it might be caused by the dominance of clay minerals in the raw coal samples (Çetinkaya and Yürüm, 2000; Georgakopoulos *et al.*, 2003; Naik *et al.*,

TABLE 3. Mineralogical compositions of studied samples based on XRD and SEM-EDS analyses (+++: dominant phase, ++: abounded phase, +: minor phase, ±: detected in few samples, a: accessory phase) (Abbreviations: Qz: Quartz, CM: Clay Minerals, Bt: Biotite, Fsp: Feldspars, Zr: Zircon, Py: Pyrite, Ccp: Chalcopyrite, Fe-Dol/Ank: Fe-Dolomite/Ankerite, Sd: Siderite, Brt: Barite, Ap: Apatite, Gyz: Goyazite)

Sample ID	Minerals														
	Qz	CM	Bt	Fsp	Zr	Py	Ccp	Cal	Fe-Dol /Ank	Sd	Brt	Ti-oxide	Fe-oxides	Ap	Gyz
SO-1		+++													
SO-2	+++	+++				a							a		
SO-3	++	+++													
SO-4	++	+++	a	a	a	+	a				a	a		a	
SO-5	+	+++				++									
SO-6	++	+++				+									
SO-7	++	+++	a			+		+							
SO-8	++	+++						++							
SO-9	++	+++						++							
SO-10	+	++						+++							
SO-11		+++						+++							
SO-12		++				a	a	+++		a					
SO-13	+	++						+++							
SO-14	++	+++				+		++							
SO-15	++	+++	a	a	a	+		+	+	a	a		a	a	a

2021). The weak and small peaks around 1425cm^{-1} might be an indicator of carbonate minerals in the samples (Çetinkaya and Yürüm, 2000). The peak at 1436cm^{-1} can be attributed to –CH3 asymmetric deformation and/or aromatic -C=C- and hydrogen-bonded O–H groups (Jiang *et al.*, 2021; Valentim *et al.*, 2013). Considering the maceral and mineralogical compositions of the samples, this peak could be related to the predominance of vitrinite macerals and the presence of clay minerals. Furthermore, the broad peak around 1610cm^{-1} appears to be an indicator of aromatic C=C and oxygen-containing functional groups, which could be related to the common presence of vitrinite and inertinite macerals in the samples (Chen *et al.*, 2013; Georgakopoulos *et al.*, 2003; Valentim *et al.*, 2013). Furthermore, the peak around 2900cm^{-1} could be related to the presence of hydrogen-rich compounds in the samples (Chen *et al.*, 2013).

Rock-Eval Pyrolysis and TOC

The S_1 and S_2 values analysed samples from the working coal seams display wide range, and measured from 1.9–3.4 and 106.0–152.6mg HC/g rock, respectively, while S_3 values are generally low and vary from 2.1 to 3.2mg CO_2/g rock (Table 4; Fig. 6A, B). The heterogeneous maceral and mineralogical compositions of the samples presumably caused variations on S_1 and S_2 values; nevertheless, low S_3 values are expected for bituminous coals due to defunctionalisation reactions of oxygen-bearing functional groups during coalification (Lo, 1993; Petersen, 2006; Uguna *et al.*, 2017; Vu *et al.*, 2013). The TOC contents of the samples ranged from 48.0% to 58.3% (Table 4). The T_{max} values were measured between 442–445ºC. The HI values were calculated between 221–288mg HC/g TOC, whereas the OI values were low, as expected, and ranged from 4 to 6mg HC/g CO_2 (Table 4). The RC and MINRC values were quite high and varied between 37.1–46.4% and 13.8–30.8%, respectively (Table 4).

Micro-Raman Spectroscopy

The Disordered (D) and Graphitic (G) bands were detected on the first-order Raman spectrum obtained from collotelinite particles of the analysed samples (Fig. 7). Notably, no second-order Raman spectra were obtained from collotelinite particles in the samples. Furthermore, lower-intensity sub-bands at approximately 1015, 1264, 1342, 1425, and 1520cm^{-1} were detected in the samples. However, these disordered sub-bands are not included in the maximum experienced temperature (T_{peak}) calculations due to their possible overlap with the G and D bands and their presence in the first-order Raman spectra of low- and medium-rank coals is still in dispute (Li *et al.*, 2020; Schito *et al.*, 2017). Hence, the Full Width at Half Maximum (FWHM) of the G band was applied for the calculation of T_{peak} in this study, according to the methodology reported in Li *et al.* (2020).

The average position of the D band of collotellinite for the samples was around 1352cm^{-1} (Table 5; Figs. 8; 9). The average D1 FWHM of collotellinite particles in

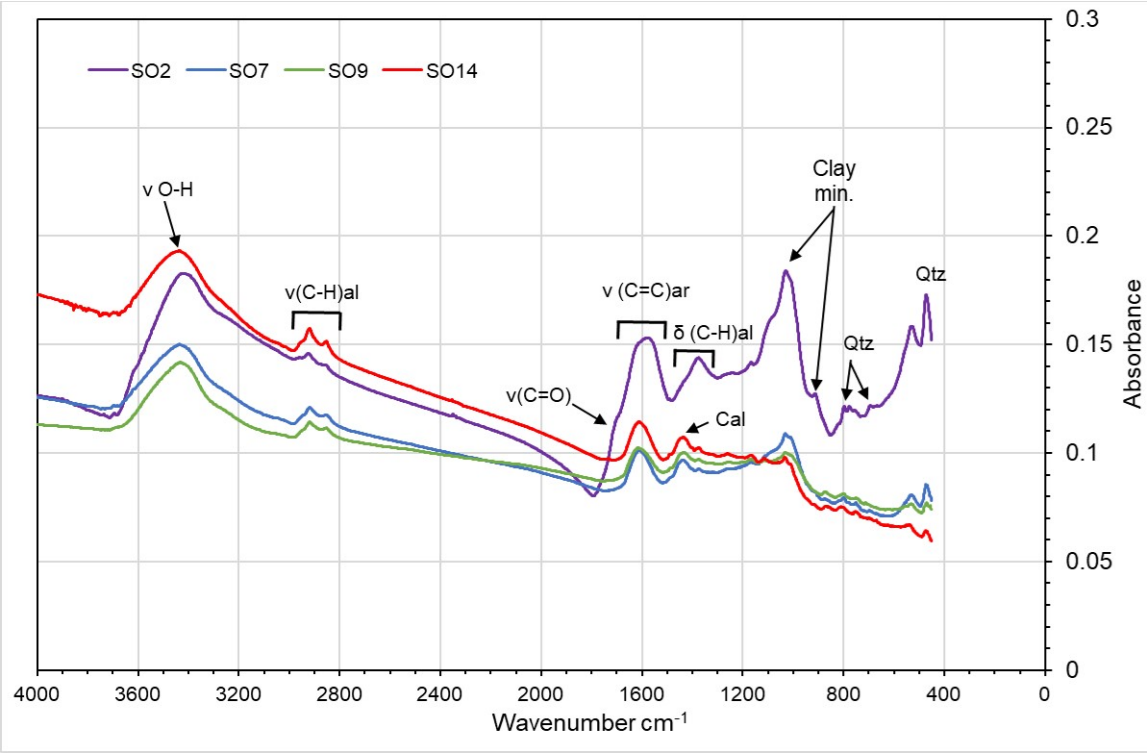

FIGURE 5. FT-IR spectra of samples SO-2, -7, -9 and -14.

the samples ranged between 90.0–92.0cm^{-1} (Table 5). The average G-band position of collotelinite particles was around 1593cm^{-1} (Figs. 7; 8). The average G FWHM values of collotelinite particles vary from 74.2 to 76.6cm^{-1} (Table 5). Finally, the D1-band vs. G-band (ID1/IG) intensity area ratio values are between 0.48 and 0.68 (Table 5). The results of micro-Raman spectroscopy analyses of collotelinite particles show that the D band appears broad, while the G band is slightly narrower, which is expected for bituminous coals. In addition, the average positions of the D and G bands are close to the reported D- and G-band positions for vitrinite particles in bituminous coal (*e.g.* Guedes *et al.*, 2010; Hinrichs *et al.*, 2014; Li *et al.*, 2020; Matlala *et al.*, 2024).

TABLE 4. The results of Rock-Eval analyses of the studied coal samples (TOC: Total Organic Carbon; HI: Hydrogen Index; PI: Production Index ((S1/(S1+S2); BI: Bitumen Index S1/TOC), QI: Quality Index ((S1+S2)/TOC); OSI: Oil Saturation Index (S1*100)/TOC))

Sample	TOC (%)	S_1 (mg HC/g rock)	S_2 (mg HC/g rock)	S_3 (mg CO_2/g rock)	T_{max} (°C)	HI (mg HC/g TOC)	OI (mg HC/g CO_2)	RC	PC	MINC	PI	QI	BI	OSI
SO-4	48.0	1.9	106.0	2.9	443	221	6	38.5	9.5	21.2	0.02	2.2	0.04	4.0
SO-5	48.8	2.5	131.3	3.2	443	269	6	37.1	11.7	30.8	0.02	2.7	0.05	5.2
SO-6	53.9	2.2	132.0	2.4	442	245	4	42.4	11.5	17.0	0.02	2.5	0.04	4.1
SO-7	53.5	2.4	131.4	2.1	443	246	4	42.0	11.4	13.8	0.02	2.5	0.04	4.5
SO-8	54.3	2.2	138.6	2.4	444	255	4	42.2	12.1	20.5	0.02	2.6	0.04	4.1
SO-9	55.4	2.9	140.2	2.1	445	253	4	43.2	12.2	16.9	0.02	2.6	0.05	5.3
SO-10	53.7	2.3	141.5	2.3	442	264	4	41.3	12.4	22.6	0.02	2.7	0.04	4.4
SO-11	56.6	3.4	146.8	2.4	442	259	4	43.7	12.9	22.5	0.02	2.7	0.06	6.0
SO-12	52.9	3.1	152.6	2.5	442	288	5	39.5	13.3	25.0	0.02	2.9	0.06	5.8
SO-13	52.5	2.8	133.3	2.2	442	254	4	40.9	11.6	19.1	0.02	2.6	0.05	5.3
SO-14	56.8	2.4	141.3	3.0	444	249	5	44.4	12.4	22.0	0.02	2.5	0.04	4.2
SO-15	58.3	2.0	136.1	2.9	442	233	5	46.4	11.9	21.5	0.01	2.4	0.03	3.5

TABLE 5. Raman parameters for Collotelinite (Ct) macerals in the analyzed samples; w-G and w-D bands positions (band center); Full-Width Half Maximum (FWHM) and intensity ratio (ID/IG)

Sample ID		w-G (cm^{-1})	G-FWHM (cm^{-1})	w-D (cm^{-1})	D-FWHM (cm^{-1})	I_D/I_G
SO-9	Ct-9/1	1591	73.7	1350	81.4	0.52
	Ct-9/2	1593	77.3	1351	97.9	0.61
	Ct-9/3	1593	72.8	1353	93.8	0.65
	Ct-9/4	1591	75.9	1353	94.8	0.61
	avg.	1592	74.9	1352	92.0	0.60
SO-7	Ct-7/1	1592	75.6	1350	83.2	0.55
	Ct-7/2	1593	73.3	1352	75.0	0.48
	Ct-7/3	1594	76.8	1352	88.6	0.54
	Ct-7/4	1592	76.7	1353	93.8	0.64
	Ct-7/5	1593	80.4	1352	109.6	0.63
	avg.	1593	76.6	1352	90.0	0.57
SO-14	Ct-14/1	1591	75.5	1352	99.7	0.68
	Ct-14/2	1593	74.4	1353	100.0	0.61
	Ct-14/3	1594	71.9	1350	86.7	0.67
	Ct-14/4	1593	69.0	1352	88.9	0.62
	Ct-14/5	1593	80.4	1352	77.2	0.48
	avg.	1593	74.2	1352	90.5	0.61

DISCUSSIONS

Rank and Geothermometer Estimation

Rank and grade determination of coal should be conducted using several coal quality parameters, such as ash yields, gross calorific values, and %Rr values (O'Keefe *et al.*, 2013), as one of these parameters can be affected by the nature of the coal seam. The studied coal samples were from both outcrop and working coal seams of bituminous C coal (medium rank-C) according to the E.C.E-U.N. (1998) chart and bituminous C according to the ISO 11760 (2018) classification. Nevertheless, the studied outcrop samples are high volatile-A bituminous coal, while working coal seam samples are high volatile-B bituminous coal, according to the ASTM D388 (2018) classification. This small difference between the outcrop and working coal seam samples is caused by the slightly higher %Rr values of the outcrop samples. Although some studies have reported that surface oxidation might cause a reduction in %Rr values and/or no changes in bituminous coals (Kruszewska and Du Cann, 1996; Mathews and Bustin, 1984), the relatively higher %Rr values of the outcrop samples were slightly increased due to surface oxidation (Kus and Misz-Kennan, 2017; Mangena and du Cann, 2007). Therefore, the outcrop samples may also be considered high volatile B, similar to the working coal seam samples. It is worth noting that the existence of epigenetic carbonate minerals cleat/fracture infillings, especially in working coal seams, might also cause the elevation of volatile matter contents and ash yields. Therefore, the ASTM D388 (2018) classification may not be an accurate rank classification for the studied seams, and it is better to classify the studied Serpukhovian–Bashkirian coals as bituminous C according to E.C.E-U.N. (1998) and ISO 11760 (2018) classifications.

In some samples, brecciated vitrinite particles have been observed, and such vitrinite macerals could be an indicator of tectonic deformation and/or influence of hydrothermal solutions (Hower *et al.*, 2001, 2021; Xie *et al.*, 2019). The existence of dykes and sills in the Zonguldak Basin has increased the coalification and caused penetration of hydrothermal solutions (Karayiğit, 1992; Karayiğit *et al.*, 2018a). Although the dykes and sills were not observed within the vicinity of the study area, the calculated T_{peak} values according to Barker and Pawlewicz's formula (T_{peak}=(lnVRr%+1.19)/0.00782) range from 117ºC to 127 ºC (Barker and Pawlewicz, 1994), which was calculated to be between 173 to 206ºC for Serpukhovian–Bashkirian coal seams in the central parts of the Zonguldak Basin (Karayiğit *et al.*, 2018a). The calculated T_{peak} values of the studied samples and the existence of cleat/fracture mineral infillings imply that circulated hydrothermal solutions might cause the formation of brecciated vitrinite particles. However, their angular morphology and variable fragment size could indicate that these particles were developed due to tectonic deformation and circulated hydrothermal solutions seemed to be precipitated after deformation (Xie *et al.*, 2019). Moreover, the influence of hydrothermal solutions on coalification might be limited due to the lack of difference in %Rr between the edges and central parts of the vitrinite particles around cleat/fracture mineral infillings (Permana *et al.*, 2013). Thus, tectonic deformation during post-coalification seems to have more influence on the coalification of the studied seams than the penetrated hydrothermal solutions.

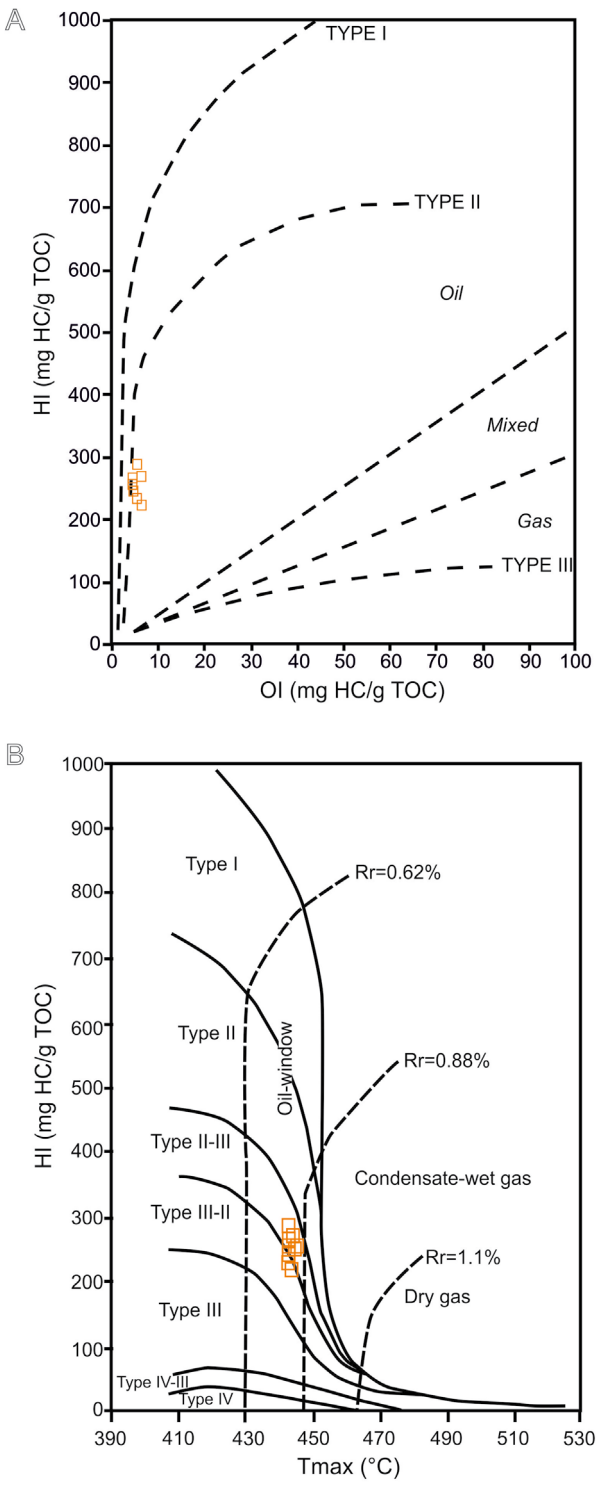

FIGURE 6. The plot of studied samples on A) pseudo-van Krveln diagram (after Peters, 1986) and B) HI-T_{max} diagram (after Peters, 1986).

The results of Raman spectroscopy could also be useful tool for calculating maximum attained temperatures of coal-bearing sedimentary sequences and organic matter-bearing rocks (Hackley and Lündsdorf, 2018; Beyssac *et al.*, 2002; Furuichi *et al.*, 2015; ; Hinrichs *et al.*, 2014; Kouketsu *et al.*, 2014; Li *et al.*, 2019, 2020). Therefore, reliable geothermometer calculations over various ranges have been proposed for high-rank coals and carbonaceous matter-bearing low-grade metamorphic rocks. These calculations are mostly based on the peak intensities of D1, D2, and G bands of vitrinite and graphite particles; however, the D2 bands of vitrinite particles in low- and medium-rank coals could not be easily observed as a shoulder next to the G band. Furthermore, the D1 band has become a more accurate parameter for high-rank coals (Hinrichs *et al.*, 2014). Therefore, using the D1 and D2 bands for geothermometer estimation of medium-rank coals could provide inaccurate results. Bolstering this, the calculated geothermometer using of the samples according to formula (T(°C)= −2.15*D1-FWHM+478) proposed by Kouketsu *et al.* (2014) for low-grade metamorphic rock is between 280.2–284.5°C. These temperatures are similar to those of thermally altered coals and are not in agreement with the %Rr and T_{max} values of the samples. Nevertheless, recent studies have shown that the G band is more reliable with rank, and using the G-FWHM for temperature determination might be more accurate for medium-rank coals (Hackley and Lündsdorf, 2018; Guedes *et al.*, 2010; Hinrichs *et al.*, 2014). Besides, the G-FWHM can also be correlated with the T_{peak} values (Guedes *et al.*, 2010; Hinrichs *et al.*, 2014). In agreement, the %Rr and G-FWHM of the samples displayed strong negative correlations (Fig. 9A). Although correlating Raman spectroscopy results could be affected by several factors, such as the polishing technique and laser beam type, another correlation is applied to obtain a more accurate estimation using calculated T_{peak} values according to %Rr and G-FWHM values of collotelinite particles with %0.69–0.81, as reported by Guedes *et al.* (2010). This correlation suggests that the calculated T_{peak} values (T_{peak}=-2.9512*G-FWHM+339.47) for the samples from the Kurtköy coalfield were between 113 and 120°C (Fig. 9B). Hence, the studied coals seem to have experienced significantly lower maximum temperatures than their counterparts in the central parts of the Zonguldak Basin. Further micro-Raman spectroscopy studies from other parts of the basin should be conducted in the future to better understand the geothermometer estimations at the basin scale.

As mentioned previously, the coal-bearing Late Carboniferous sequences in the basin experienced several orogenic movements during the Late Palaeozoic (Variscan orogeny) and Late Mesozoic–Cenozoic (Alpine orogeny). Thus, coal-bearing Late Carboniferous sequences were deformed and thrusted over during post-coalification, particularly in the central (*e.g.* Kozlu and Karadon coalfields) and eastern parts (*e.g.* Amasra coalfield) of the basin. Furthermore, the coal seams in the northern parts of the Zonguldak Basin have deeper recent burial depths than

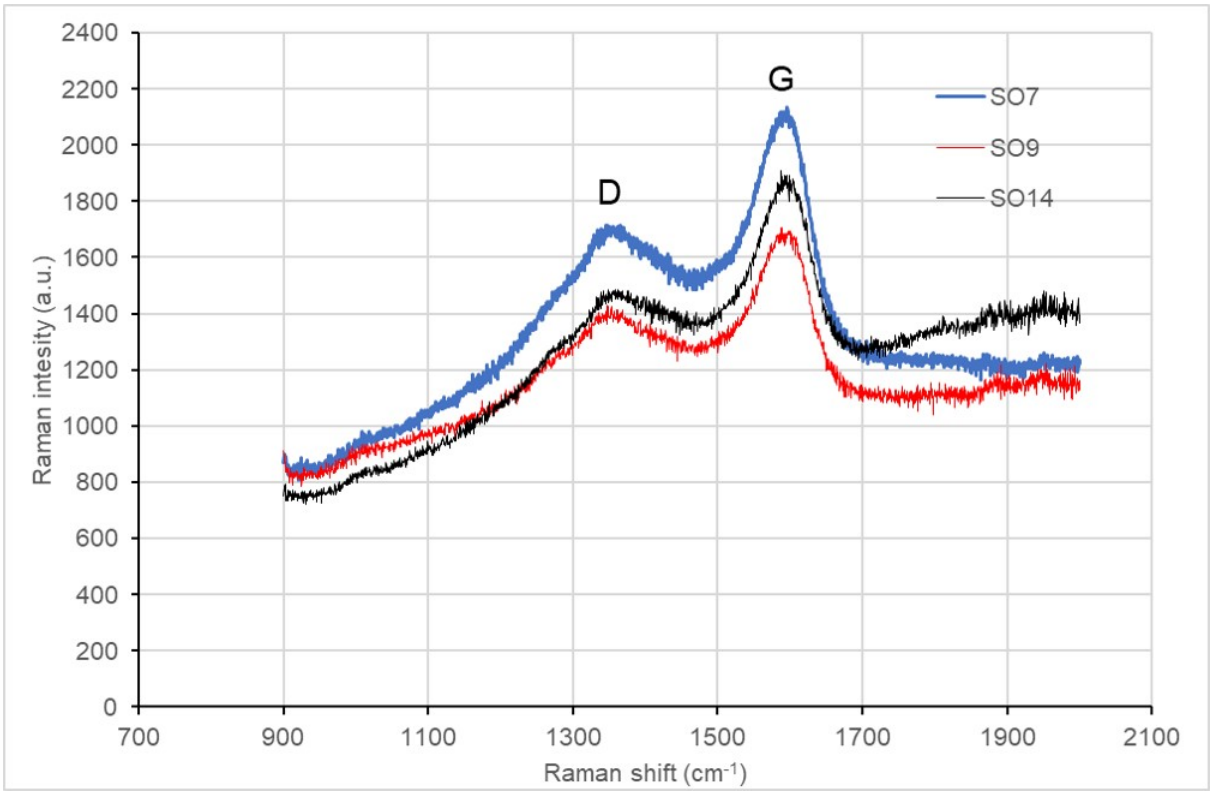

FIGURE 7. Representative micro-Raman Spectra for collotellinite grains from samples SO-7, -9 and -14. Baseline not corrected.

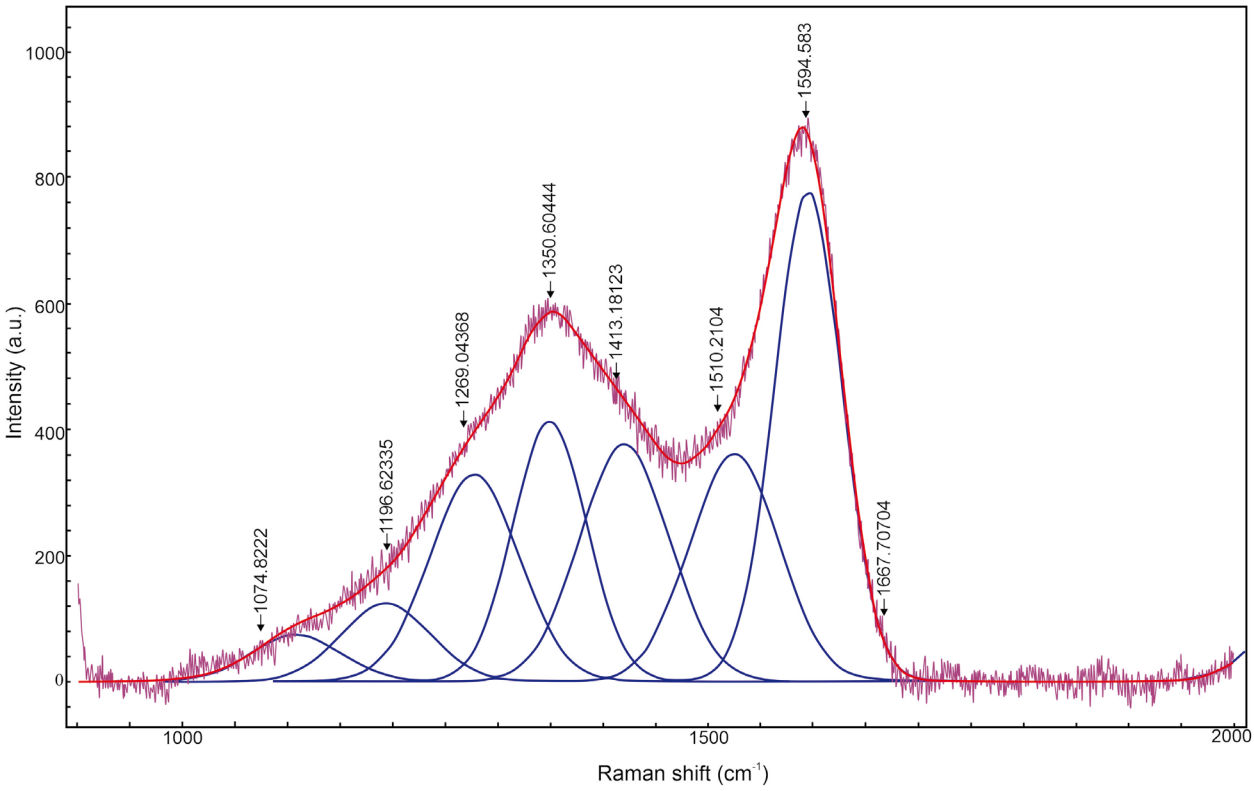

FIGURE 8. Representative micro-Raman spectra of collotellinite grain from SO-7; fitted and baseline corrected.

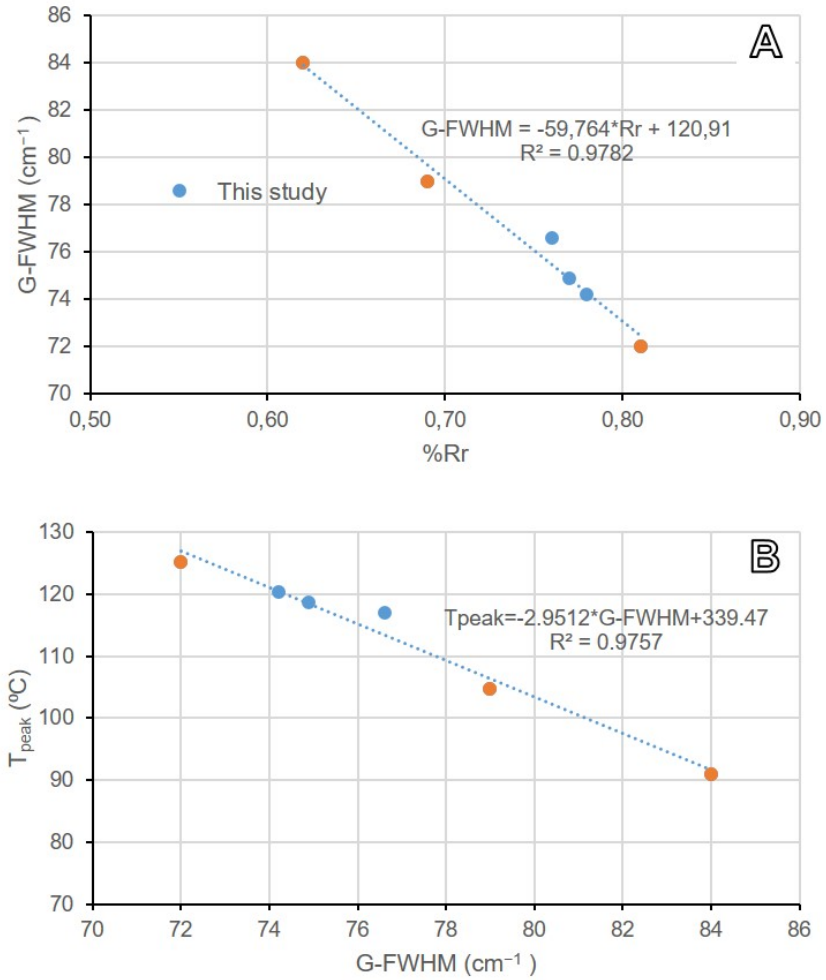

FIGURE 9. Correlations between A) G-FWHM (cm^{-1}) vs. %Rr and B) G-FWHM (cm^{-1}) and calculate T_{peak} values using %Rr data.

those in the southern and South-eastern parts of the basin, where the studied coalfield is located (Karayigit, 1992, 2001, 2003). As expected, the reported %Rr values of the Serpukhovian–Bashkirian coal seams in the Alacaağzı Fm. from the northern parts of the Zonguldak Basin range between 1.18–1.52% (Karayiğit, 1992; Karayiğit *et al.*, 2018a, 2018b; Yalçin *et al.*, 2002). As a result, the rank of Serpukhovian–Bashkirian coal seams in the northern parts of the Zonguldak Basin is generally higher than those of other coal-bearing formations in the basin. Nevertheless, the %Rr values of the studied Serpukhovian–Bashkirian coals indicate that the degree of coalification is significantly lower than that of their counterparts in the northern parts of the basin. Furthermore, the %Rr values of the studied Serpukhovian–Bashkirian coals are close to those of the Duckmantian–Asturian coal seams (Karadon Fm.) in the northern parts of the Zonguldak Basin and the Langsettian coal seams (Kozlu Fm.) in the Amasra coalfield (Karayiğit, 1992; Karayigit *et al.*, 1998, 2018b; Yalçin *et al.*, 2023). Overall, the studied coal seams-bearing Serpukhovian–Bashkirian sequences presumably were not severely affected by the Alpine Orogeny than the other Serpukhovian–Bashkirian coal seams in the basin. Therefore, the studied Serpukhovian–Bashkirian coals have relatively shallow recent burial depths and lower degree of coalification than their counterparts in the basin. This data also implies that the tectonic deformation and heat flow of coal-bearing sequences in the Zonguldak Basin might not be similar across the entire basin.

Provenance of Minerals

The mode of occurrence of minerals in coal could be useful for the estimation of depositional conditions, sediment input source area during peat accumulation, and the chemistry of circulated fluids within coal seams during coalification (Ward, 2002; Dai *et al.*, 2020). Although determining the timing of mineral formation

and emplacement is challenging, the petrographic and SEM-EDS data of the samples imply that the identified minerals seem to be mainly derived from clastic and/or contemporaneous volcanic inputs and authigenic precipitation within palaeomires and/or during peatification (syngenetic), and coalification and weathering processes (epigenetic).

Quartz and clay minerals, particularly kaolinite, were the most commonly detected minerals in the samples. The SEM-EDS observations showed that quartz/silica and feldspar grains were mostly identified as individual grains within the clay mineral matrix (Fig. 10). Such individual grains within the clay mineral matrix are generally related to clastic inputs into palaeomires and/or epiclastic and/or contemporaneous volcanic inputs in the Zonguldak Basin (Bohor and Triplehorn, 1993; Dai *et al.*, 2017, 2020; Ward, 2002, 2016). Previous studies from the Late Carboniferous coal seams and coal-bearing sequences from the central parts of the Zonguldak Basin showed that quartz/silica, feldspars, apatite, biotite, chlorite, Ti-oxides, and zircon grains were also commonly observed within kaolinitic matrices and rarely within illitic matrices (Karayiğit *et al.*, 2018a, b). The former associations within kaolinitic matrices have also been identified in the tonstein layers of the Amasra and Zonguldak coalfields (Burger *et al.*, 2000; Karayiğit *et al.*, 2022). Considering the co-existence of quartz and feldspar grains with biotite, chlorite, Ti-oxides, and zircon within the kaolinitic matrices of the studied samples, they were mainly derived from contemporaneous and/or epiclastic volcanic inputs into the paleomire during the Late Carboniferous. Nevertheless, quartz/silica grains within illitic matrices also imply that quartz/silica could be derived as clastic inputs from pre-Carboniferous basements. As mentioned above, kaolinite is mostly identified as a matrix of clay mineral aggregates and, to a lesser extent, as vermicular grains during SEM-EDS studies (Fig. 10B, C). Such occurrences have also been reported in tonstein layers within Late Carboniferous coal seams and sequences (Burger *et al.*, 2000; Karayiğit *et al.*, 2022). It is well documented that when contemporaneous and/or epiclastic volcanic inputs were altered within palaeomires, their alteration by-products could be variable depending on the pH of mire water and/or hydrogeological conditions (Bohor and Triplehorn, 1993; Dai *et al.*, 2017). The existence of kaolinitic matrices and vermicular kaolinite grains is generally related to weak acidic to neutral conditions under open hydrogeological conditions. In such conditions, liberated ions, except Al^{3+} and Si^{4+}, from alterations of volcanic inputs (*e.g.* air-fall ash or tephra) and/or epiclastic volcanic inputs were prone to transfer to outside of mire conditions, and kaolinitic matrices and vermicular kaolinite grains were authigenically precipitated from Al- and Si-rich solutions within the palaeomires and/or during peatification (Dai *et al.*, 2017; Spears, 2012). This could also explain the lack of characteristic bands for kaolinite in the FT-IR spectra of the samples, which implies disordered nature for kaolinite and epiclastic volcanic input origin (Zhao *et al.*, 2012). Thus, kaolinite in the studied samples could have syngenetic origin. Furthermore, cell-lumen and cleat/fracture kaolinite infillings were also identified during the SEM-EDS studies (Figs. 11A; 12A, D), implying that kaolinite could also be derived from the precipitation of Al- and Si-rich pore water during the late stages of peatification and/or circulated hydrothermal fluids during coalification. Hence, kaolinite also has partial epigenetic origin in the samples.

Chlorite and illite were the other clay minerals detected in the samples. The SEM-EDS data indicate that chlorite is observed as lath-shaped grains (Fig. 10A) and rarely as cell-lumens infillings (Fig. 11C, D). Furthermore, chlorite grains in the samples were Fe-rich (chamosite). Lath-shaped chlorite grains are presumably related to the alteration of contemporaneous and/or epiclastic volcanic inputs, while cell-lumen infillings are presumably the precipitation of Fe-, Mg-, and Si-rich pore water during the late stages of peatification and/or the late diagenetic stages. On the other hand, the lack of NH_4-illite and pyrophyllite within cell lumen infillings, according to the SEM-EDS data, suggested that the circulating fluids did not reach either sufficient temperature or were Si-rich to convert cleat/fracture kaolinite infillings into chlorite, NH_4-illite, and pyrophyllite (Zhao *et al.*, 2018). Therefore, cell lumen chlorite infillings in the samples seem to have developed from circulating pore waters within seams and precipitated during the late diagenetic stages and/or initial stages of coalification.

Illite in the samples comprised matrices of clay mineral aggregates (Fig. 10A, B, D) and is generally considered as clastic input into palaeomires (Siavalas *et al.*, 2009; Ward, 2002). In the studied samples, the SEM-EDS data showed that the illitic matrices were presumably not pure mica. Similar observations were also reported in detailed clay mineralogy studies from Late Carboniferous coal-bearing sequences in the Zonguldak coalfields (Karayiğit, 1991; Karayiğit *et al.*, 2022) and illites in the Late Devonian–Early Carboniferous (Tournisian–Visean) Yılanlı Fm. have compositions similar to phengite and/or muscovite (Bozkaya *et al.*, 2016). The detailed clay mineralogy along with oxygen ($\delta^{18}O$) and H (δD) isotope data from Devonian–Early Carboniferous illites suggested that illitization of K-bentonite occurred during the Variscan and Cimmerian orogenies (Permian to Early Jurassic). However, illite and interstratified Illite/Smectite (I/S) in Late Carboniferous coal seams and clayey sedimentary rocks seem to have originated from clastic inputs and the transformation of detrital interstratified clay mineral matrices into I/S during diagenesis (Arostegui *et al.*, 2019; Deon *et al.*, 2022; Karayiğit *et al.*, 2022).

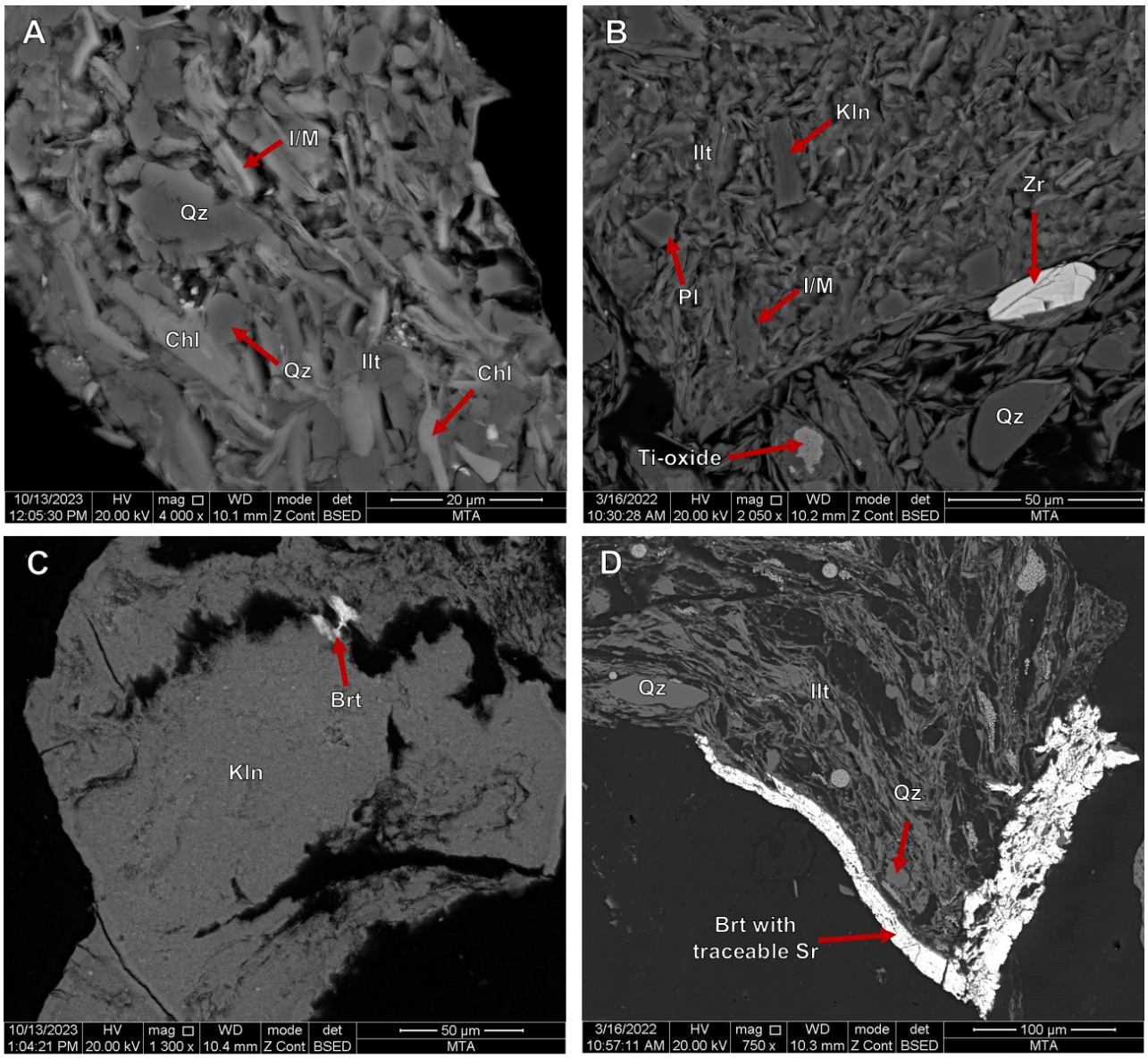

FIGURE 10. SEM backscattered images of crystalline (SEM-BSE) phases in the studied samples (A and C from SO-15 and B and D from SO-4). A) Chlorite (Chl), Illite/Mica (I/M) and Quartz (Qz) grains associated with Illitic (Ilt) clay aggregate; B) Kaolinite associated with illite, illite/mica, plagioclase, quartz, Ti-oxide and zircon granis; C) Kaolinitic aggregate and barite; D) Quartz grains associated with illitic clay aggregate, and epigenetic barite with traceable Sr. (Abbreviations: Brt: Barite, Ilt: Illite, I/M: Illite/Mica, Kln: Kaolinite, Pl: Plagioclase, Qz: Quartz, Zr: Zircon).

Nevertheless, burial depths and palaeotemperatures of the coal seams should be between 2400 and 3700m and 120–160°C, respectively, for a such transformation. Considering the calculated T_{peak} temperature of working coal seams and the minor existence of I/S in the XRD-clay fraction, the studied coal seams did not reach either sufficient burial depths and/or paleotemperature for I/S transformation, like the other Late Carboniferous coal seams in the central parts of the Zonguldak Basin. This is also evident from the significantly lower degree of coalification in comparison with the other Serpukhovian–Bashkirian coal seams in the central parts of the Zonguldak Basin. These results suggest that the studied Serpukhovian–Bashkirian coals could not reach sufficient heat flow and/or burial depths in order to transform interstratified clay mineral matrices into I/S during coalification. This might also be another piece of evidence for the samples, presumably not affected densely by orogenic movements after the Permian in the Zonguldak Basin. Thus, they did not experience high heat flows, similar to other Late Carboniferous coal seams in the central parts of the basin.

Possible Mn-bearing illitic matrices were also observed in the outcrop samples during the SEM-EDS studies (Fig.

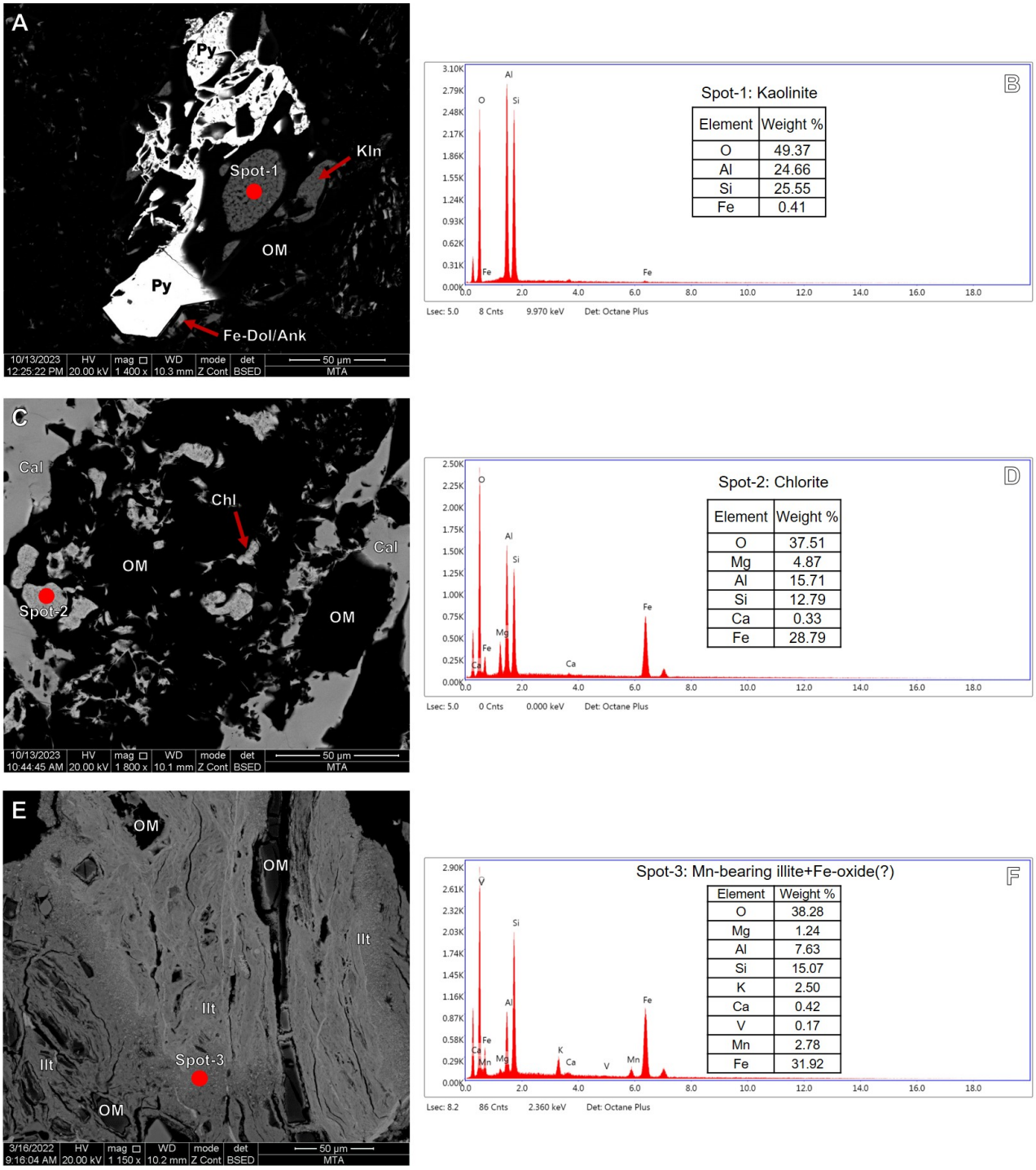

FIGURE 11. SEM backscattered images of crystalline (SEM-BSE) phases in the studied sample (A and C from SO-15 and E from SO-2). A) Cleat/fracture pyrite and Fe-dolomite/ankerite infillings, and cell-lumen kaolinite infillings; B) SEM-EDX spectra of kaolinite at spot-1 in image A; C) Cleat/fracture calcite infillings, and cell lumen chlorite infillings; D) SEM-EDX spectra of chlorite at spot-2 in image C; E) Mn-bearing illite with possible Fe-oxide intrusion; F) SEM-EDX spectra of Mn-bearing illite and Fe-oxide at spot-3 in image E (Abbreviations: Cal: Calcite, Chl: Chlorite, Fe-Dol/Ank: Fe-Dolomite/Ankerite, Ilt: Illite, Kln: Kaolinite, OM: Organic Matter, Py: Pyrite).

11E, F). Such high Mn-bearing illitic matrices have not been previously reported from coal seams in the Zongludak Basin. Nevertheless, Mn-bearing illite matrices have been reported in altered coal seams and sediments of coal mine ponds. Since illite has Mn exchange capacity, the liberated Mn^{2+} from the alteration of Mn-bearing minerals (*e.g.*

euhedral pyrite grains) can be taken up by illitic matrices (Bansal, 1983; Larsen and Mann, 2005; van Groeningen *et al.*, 2020; Wang *et al.*, 1993). Considering the presence of oxidized pyrite grains and Fe-oxides in the outcrop samples, the Mn^{2+} ions liberated from the surface weathering of pyrite grains might be taken up by illitic matrices during surface weathering.

Carbonate minerals in the samples were generally calcite, while Fe-bearing dolomite, ankerite, and siderite were rarely identified during the SEM-EDS studies (Table 3). In addition, carbonate minerals were mostly observed as cleat/fracture infillings (Figs. 12C; 13A–D; 14), and, to a lesser extent, cell-lumen infillings (Fig. 13E, F). Such infillings are generally related to the precipitation of Ca- and Mg-rich hydrothermal fluids and/or circulating pore water within coal seams (Dawson *et al.*, 2012; Ward, 2016). Similarly, cleat/fracture carbonate infillings have also been reported in the Late Carboniferous coal seams in the Zonguldak Basin (Karayiğit *et al.*, 2018a, b). The SEM-EDS data also showed that calcite contained measurable amounts of Mn and Fe. The sources of Ca, Mg, Fe, Mn, and CO_2 in circulating fluids within the studied coal seams might be hydrothermal solutions in the basin; however, cleat/fracture carbonate infillings were mostly observed within the brecciated vitrinite particles, and no magmatic dykes and sills were reported from the vicinity of the study area. Nevertheless, tectonic deformation during and/or after coalification could also allow the penetration of leached solutions from overlying Mesozoic carbonates into the studied coal seams (Dawson *et al.*, 2012; Xie *et al.*, 2019); hence, cleat/fracture carbonate infillings are presumably mainly derived from the precipitation of Ca, Mg, Fe, and Mn-bearing solutions from penetrated hydrothermal solutions and/or leached solutions from overlying Mesozoic carbonates via faults in the study area. Cell-lumen carbonate infillings, on the other hand, were mostly pure $CaCO_3$ and rarely Fe-dolomite/ankerite; therefore, these infillings were presumably formed from the precipitation of Ca-rich pore waters during the late peatification and/or late diagenetic stages. Siderite micronodules have been commonly reported in the Late Carboniferous coal seams and coal-bearing sediments in the Zonguldak Basin (Karayiğit *et al.*, 2018a, b, 2022); contrary, siderite was only detected as cleat/fracture infillings in the samples (Figs. 113D;14E, F). The lack of syngenetic siderite micronodules in the studied samples could be an indicator of relatively lower pH conditions in the paleomires (Passey, 2014; Shen *et al.*, 2023); in turn, syngenetic carbonate mineral precipitation in the paleomires was limited. Overall, the carbonate minerals in the samples mainly have an epigenetic authigenic origin and a minor syngenetic authigenic origin.

Pyrite was the only sulphide mineral detected in the samples, whereas chalcopyrite was also an accessory sulphide mineral phase in the samples (Table 3). Clustered bodies of framboidal pyrite grains along with individual framboidal pyrite grains were commonly observed in

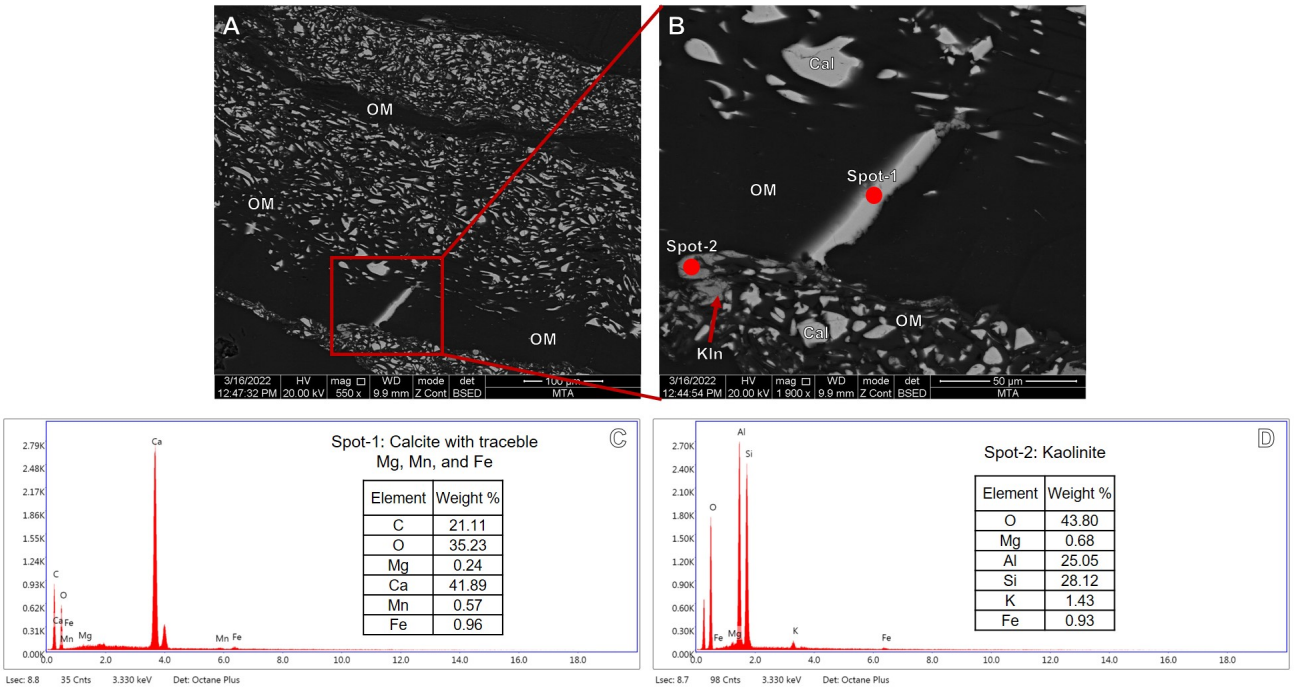

FIGURE 12. SEM backscattered images of crystalline (SEM-BSE) phases in sample SO-12. A) Cleat/fracture calcite infilling and cell-lumen calcite and kaolinite infillings; B) Enlarged image of selected area in image a; SEM-EDX spectra of C) Cleat/fracture calcite infilling at spot-1 and cell lumen kaolinite infilling at spot-2 in image C (Abbreviations: Cal: Calcite, Kln: Kaolinite, OM: Organic Matter).

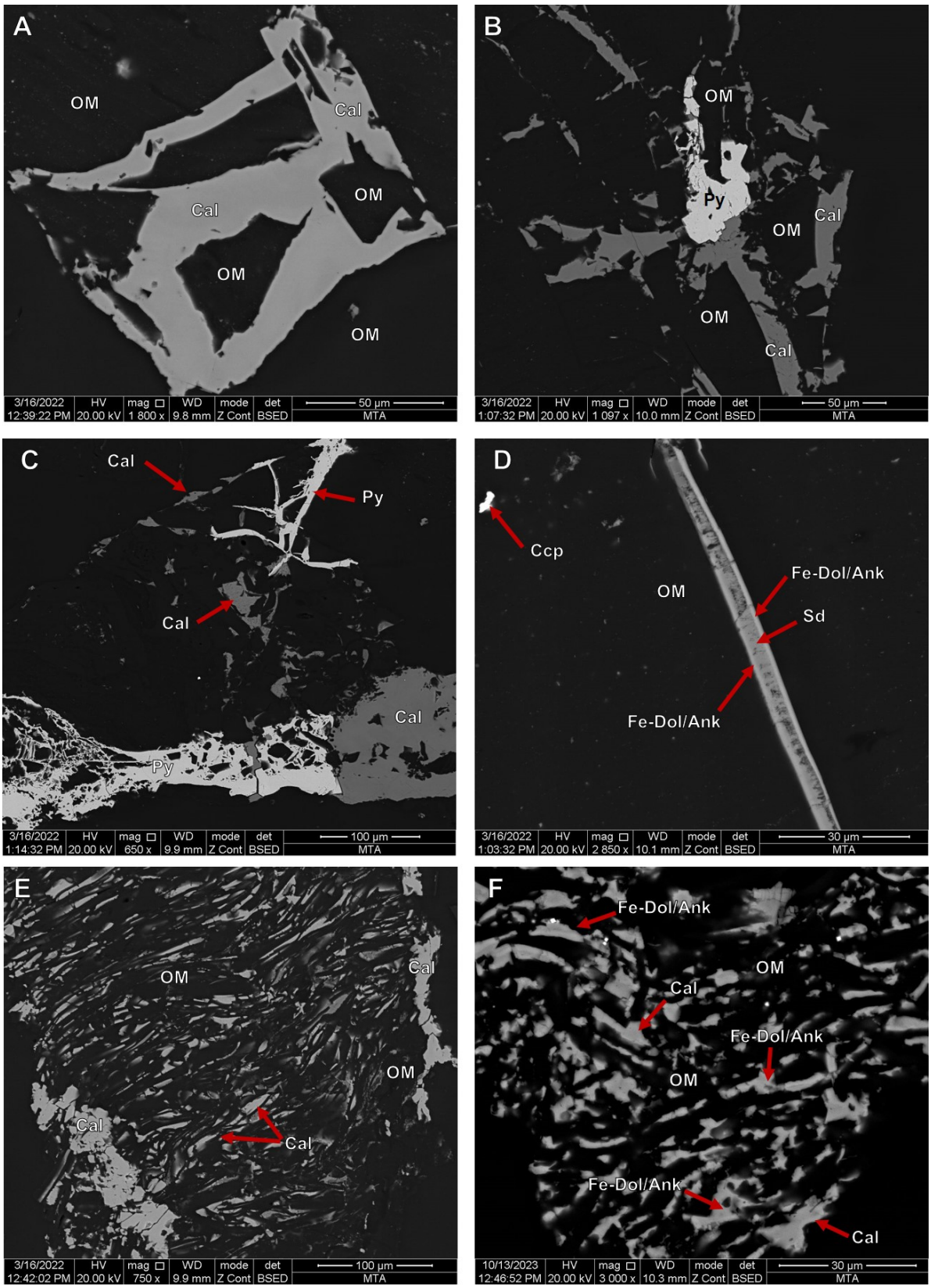

FIGURE 13. SEM backscattered images of crystalline (SEM-BSE) phases in the studied samples (A, C, D and F from SO-12, and B and E from SO-15).; A-C) Cleat/fracture calcite and pyrite infillings within brecciated vitrinite grains; D) Cleat/fracture chalcopyrite, Fe-dolomite/ankerite and siderite infillings; E-F) Cell lumen calcite and Fe-Dol/Ank infillings (Abbreviations: Cal: Calcite, Ccp: Chalcopyrite, Fe-Dol/Ank: Fe-Dolomite/Ankerite, OM: Organic Matter, Py: Pyrite, Sd: Siderite).

both outcrop and working coal seam samples during the SEM-EDS studies (Fig. 15A, B), and cleat/fracture pyrite infillings are also observed in the working coal seam samples (Figs. 13B, C; 14A, C, E; 16). These observations show that framboidal pyrite grains in the studied samples were formed authigenically under anoxic conditions within the paleomires and/or early diagenetic stages. Besides, cleat/fracture pyrite infillings were commonly reported in the Late Carboniferous coal seams in the basin (Karayiğit *et al.*, 2018a, b). These cleat/fracture infillings seem to have formed during the epigenetic stages due to the precipitation of Fe- and sulphate-rich hydrothermal fluids and/or circulating pore waters within coal seams. Their co-occurrence with epigenetic carbonate minerals in brecciated vitrinite grains (Figs. 13E; 15D; 16D) and calculated T_{peak} temperatures imply that the source of sulphate-rich solutions could originate from both penetrated hydrothermal solutions and/or leached solutions during the deposition of Mesozoic marine carbonates via faults in the study area. In addition, the rare existence of oxidised pyrite grains and pyrite relicts with Fe-oxide and Fe-sulphate compositions in the outcrop samples (Fig. 15C), cleat/

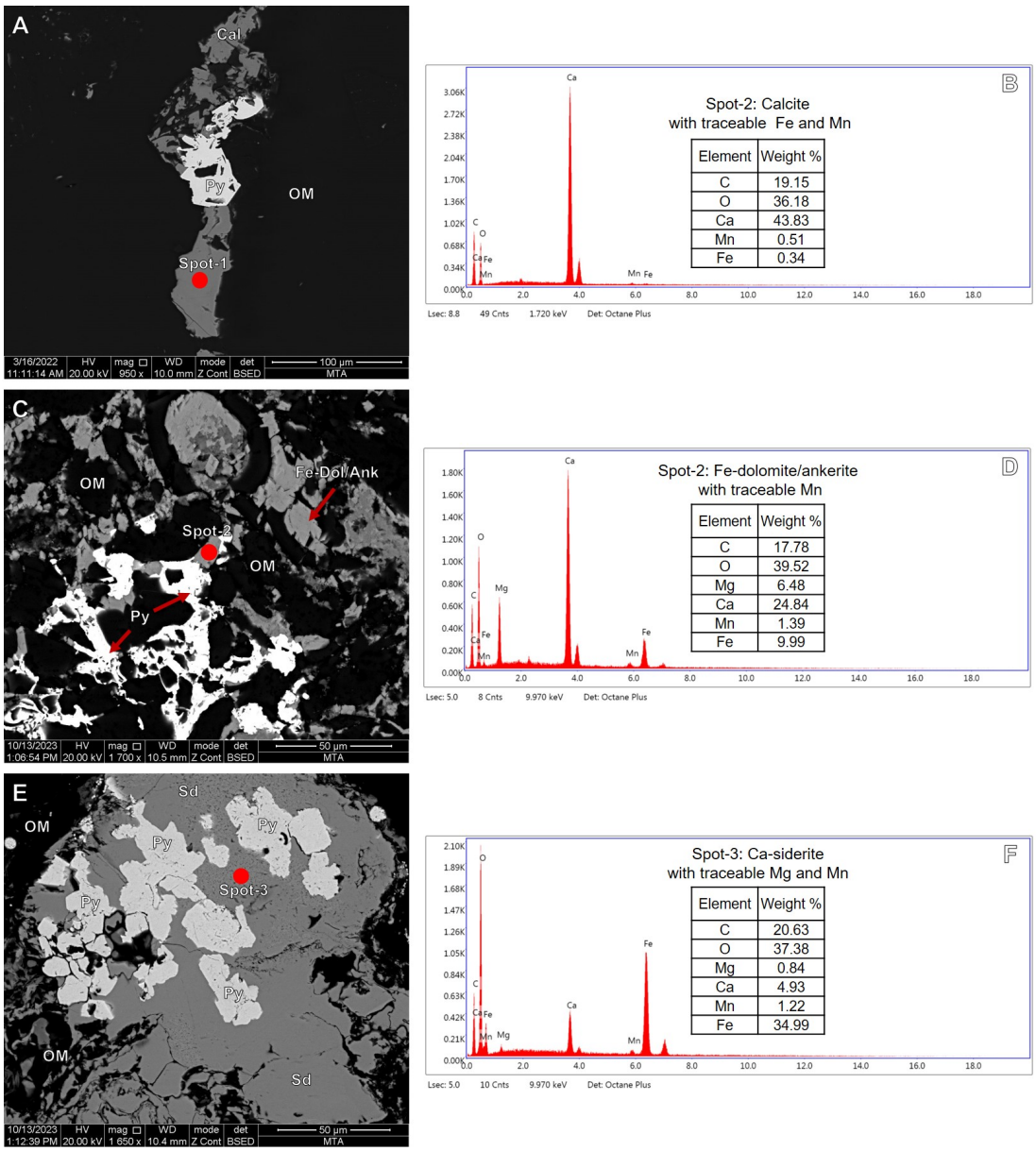

FIGURE 14. SEM backscattered images of crystalline (SEM-BSE) phases in the studied samples (A from SO-12, and C and E from SO-15). A) Cleat/fracture calcite and pyrite; B) SEM-EDX spectra of cleat/fracture calcite infilling at spot-1 in image A; C) Cleat/fracture Fe-dolomite/ankerite and pyrite infillings; D) SEM-EDX spectra of cleat/fracture Fe-dolomite/ankerite infilling at spot-2 in image C; E) Cleat/fracture siderite and pyrite infillings; F) SEM-EDX spectra of cleat/fracture siderite infilling at spot-3 in image E (Abbreviations: Cal: Calcite, Fe-Dol/Ank: Fe-Dolomite/Ankerite; OM: Organic Matter; Py: Pyrite and Sd: Siderite).

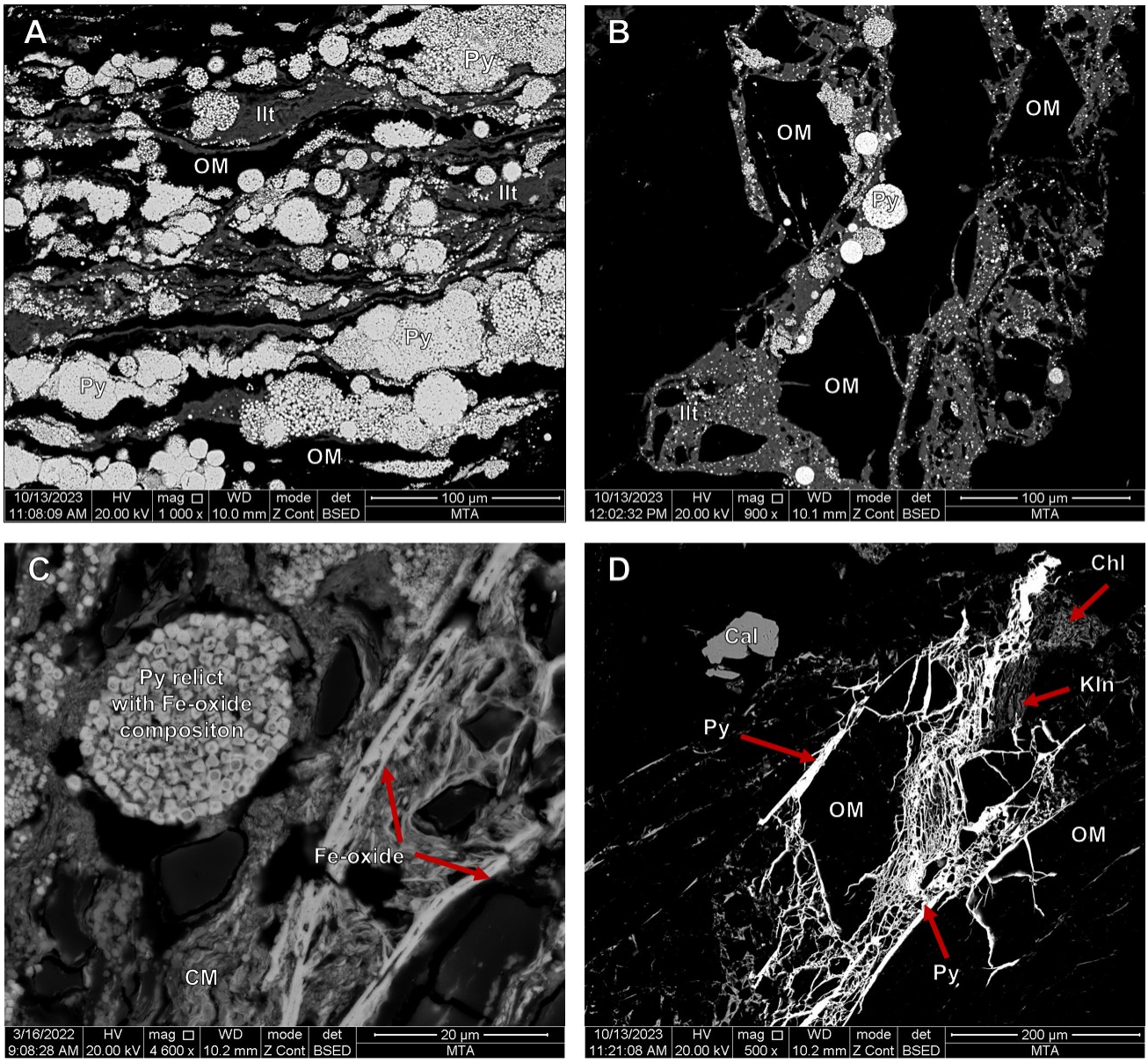

FIGURE 15. SEM backscattered images of crystalline (SEM-BSE) phases in the studied samples (A and C from SO-7, B from SO-15, C from SO-2). A-B) Framboidal pyrite grains associated with illite and organic matter; C) Pyrite relict with Fe-oxide composition with clay mineral aggregates and Fe-oxide cleat/fracture infillings; D-E) Cleat/fracture pyrite and calcite infillings, and cell-lumen kaolinite () and chlorite infillings (Abbreviations: Cal: Calcite, Chl: Chlorite, CM: Clay Minerals, Ilt: Illite, Kln: Kaolinite, OM: Organic Matter, Py: Pyrite).

fracture Fe-oxide infillings, and honeycomb-like Fe-oxide nodules also indicate that source Fe and sulphate ions might also be leached solutions from oxidised sulphide minerals. Nevertheless, their contributions could be very limited since there is a possibility that the oxidation of sulphide minerals might have formed more recently. Chalcopyrite was detected as individual grains within organic matter and/or clay mineral matrix during SEM studies (Fig. 13D). These observations show that chalcopyrite is derived as clastic input from epiclastic and/or contemporaneous volcanic inputs within the palaeomires.

Barite was the only identified sulphate minerals in the samples during the SEM-EDS studies. As mentioned above, Fe-sulphate composition pyrite relicts were also observed in the outcrop samples during the SEM studies (Fig. 15C), which were formed from the surface oxidation of framboidal and single-crystal pyrite grains. Barite was observed as cleat/fracture (Fig. 10C, D) and contained measurable amounts of Sr and Fe by SEM-EDS. This mode of occurrence is mostly related to the epigenetic precipitation of Ba- and sulphate-bearing hydrothermal solutions and/or circulating pore water within coal seams

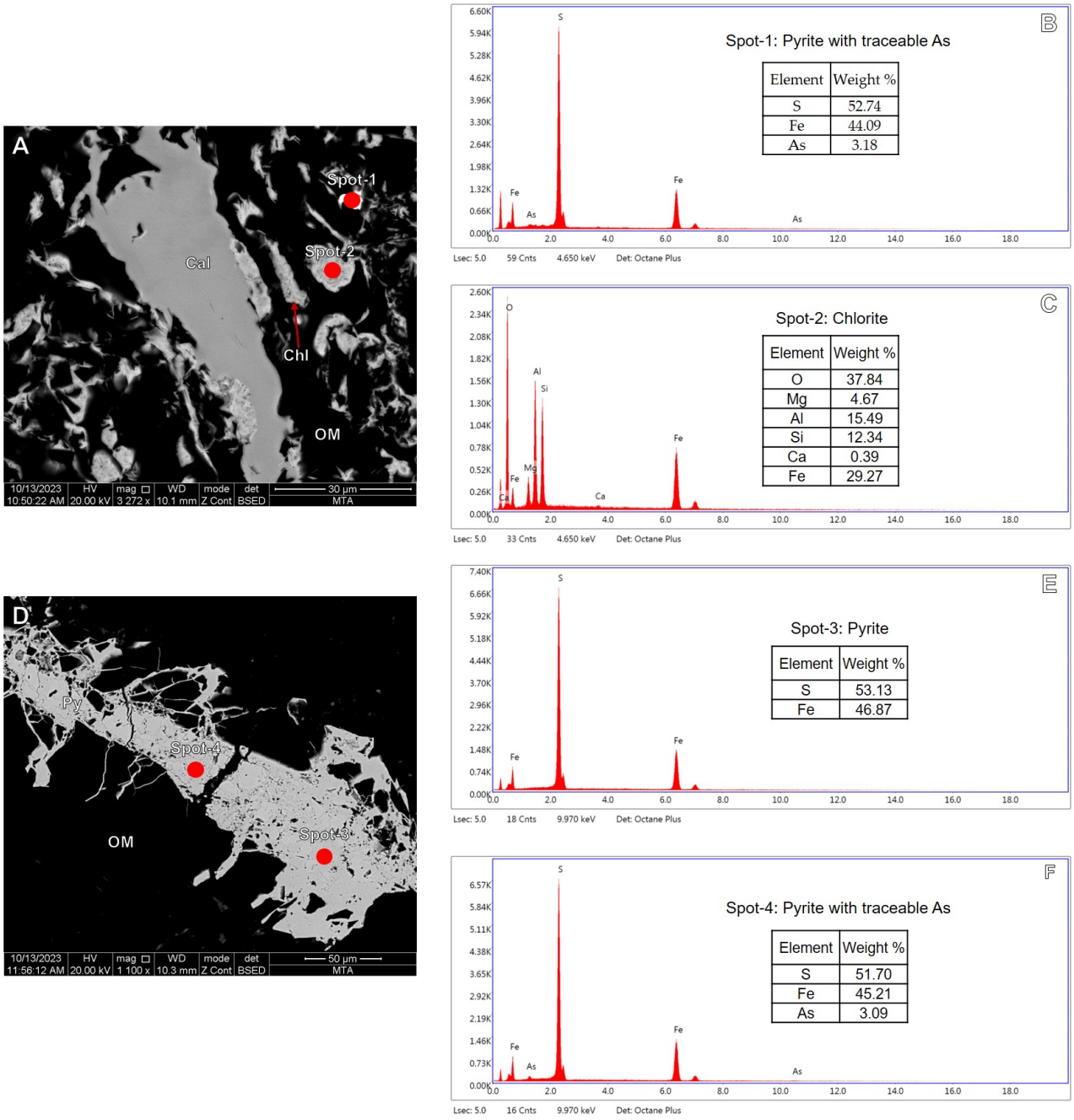

FIGURE 16. A, D) SEM backscattered images of crystalline (SEM-BSE) phases in the studied samples (A from SO-7 and D from SO-15). SEM-EDX spectra of B) pyrite with traceable As at spot-1 in image A. C) Cell-lumen chlorite infilling at spot-2 in image A. E) Cleat/fracture pyrite infilling at spot-3 in image D. E) Cleat/fracture pyrite with traceable As at spot-4 in image D (Abbreviations: Cal: Calcite, Chl: Chlorite, OM: Organic Matter).

(Dawson *et al.*, 2012; Zhou *et al.*, 2022). Moreover, the liberated Ba^{2+} and Sr^{2+} ions from the alteration of feldspar grains within clay mineral matrices during the late diagenetic stages could also be another source (Çelik *et al.*, 2021), which could also explain the existence of Sr-bearing barite cleat/fracture-infillings around clay mineral matrices in the studied samples. Although the paragenesis of cleat/fracture barite infillings could be variable, barite seems to have formed from authigenic precipitation during the late diagenetic and/or more possibly epigenetic stages.

Besides apatite, REE-bearing goyazite is another phosphate mineral identified during the SEM-EDS studies (Fig. 17A, B). Although it was detected in one sample (SO-15), goyazite-gorceixite-crandallite group minerals in coal could be related to the low pH or water table within the

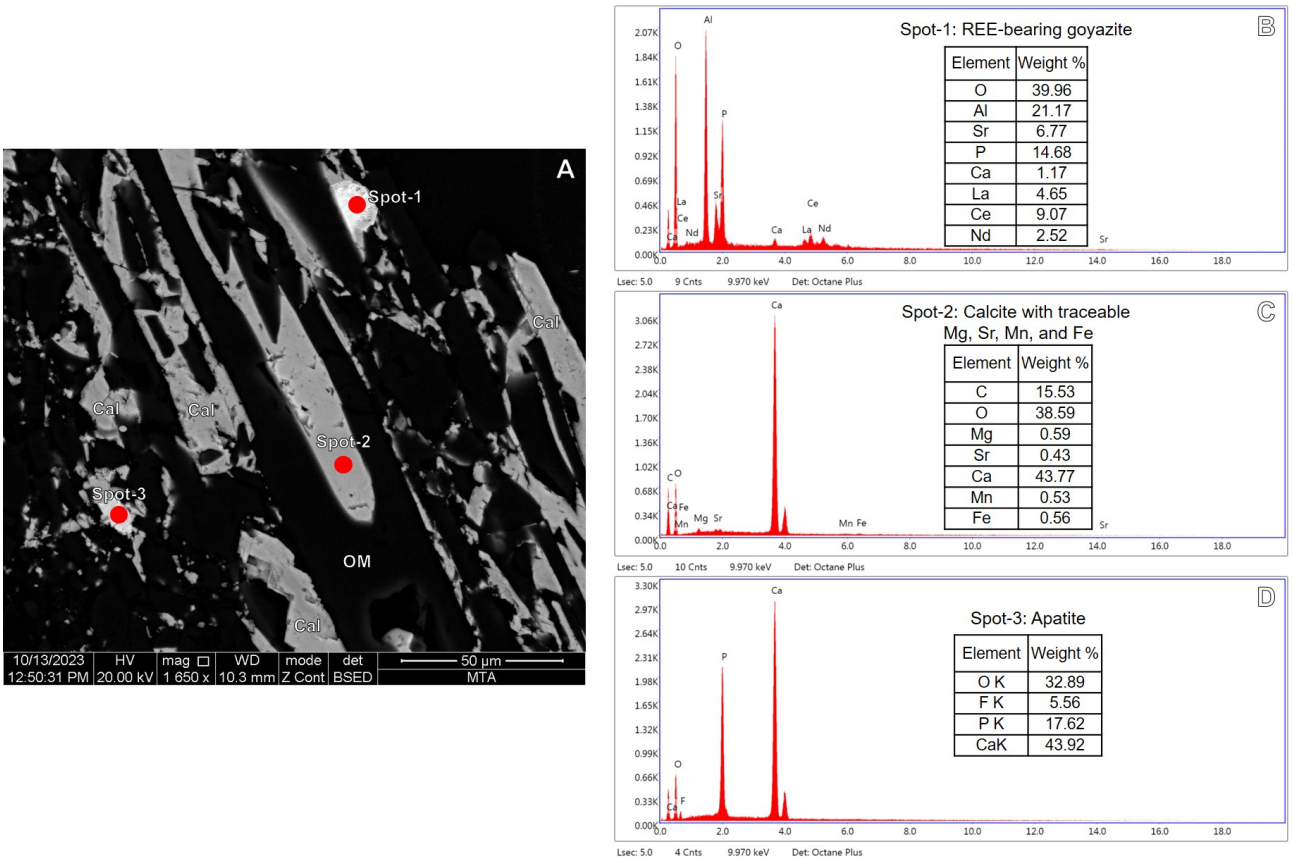

FIGURE 17. A) SEM backscattered images (SEM-BSE) of cell-lumen infillings from sample SO-15. SEM-EDX spectra of B) REE-bearing goyazite at spot-1, C) calcite with traceable Mg, Sr, Mn and Fe at spot-2 and D) apatite at spot-3 (Abbreviations: Cal: Calcite, OM: Organic Matter).

palaeomires under oxic conditions (Dai *et al.*, 2015, 2020). Previous studies from the Late Carboniferous seams have not reported the presence of goyazite-gorceixite-crandallite to date, which might suggest that the palaeomires of the studied seams may have experienced short-term oxidation or low water table conditions. The relatively high total inertinite content of the samples also supports this assumption; however, previous palynological studies from the Serpukhovian–Bashkirian coal seams in the Zonguldak Basin reported humic climatic conditions during peat-forming periods (Akgün and Akyol, 1992).

Furthermore, the existence of inertodetrinite and fusinite macerals within the humic matrix of collodetrinite could suggest an allochthonous origin of inertinite macerals (Dai *et al.*, 2020; Scott and Glasspool, 2007). Nevertheless, goyazite-gorceixite-crandallite group minerals could also form reactions between Al, Ca, and P, which were leached from the alteration of contemporaneous and/or epiclastic volcanic inputs within the palaeomires under pH conditions between 3.3 and 4.6 (Bohor and Triplehorn, 1993; Rao and Walsh, 1997, 1999). Taking into account that tonstein layers within the Late Carboniferous coal seams in the Zonguldak Basin are commonly observed, and the presence of REE-bearing goyazite in tonstein layers (Burger *et al.*, 2000; Karayiğit *et al.*, 2022), REE-bearing goyazite in sample SO-15 seems to have been formed by reactions between liberated Al and P from the alteration of contemporaneous and/or epiclastic volcanic inputs during peatification under acidic conditions. This could also explain its co-existence within apatite and calcite cell-lumen infillings in sample SO-15 (Fig. 17A, C, D).

Polymineralic infillings were commonly reported from other Late Carboniferous coal seams in the Zonguldak Basin and displayed similar mineral paragenesis with hydrothermally affected coal seams (Karayiğit *et al.*, 2018a, b), whereas monomineralic infillings were more common in the samples. The SEM-EDS observations show that monomineralic cleat/fracture infillings are mostly composed of carbonate minerals and pyrite and, to a lesser extent, kaolinite, chlorite, and barite (Figs. 10C, D; 11A, C; 12B; 13A; 16A, D), while polymineralic cleat/fracture infillings are mainly composed of pyrite-carbonate minerals (mostly calcite, and rarely Fe-dolomite/ankerite siderite) associations (Figs. 13B, C; 14A, C, E) and rarely Fe-dolomite/ankerite-siderite associations (Fig. 13D). Monomineralic kaolinite and chlorite cell-lumen and

cleat/fracture infillings (Figs. 11A; 12B; 16A, C) could imply that these infillings seem to have been developed from the precipitation of Al and Si-bearing circulated fluids during the late diagenetic stages and/or epigenetic stages. However, the presence of kaolinite and chlorite monomineralic infillings within the organic matter could also suggest that the precipitation of Al-, Mg-, and Si-rich circulated fluids within the palaeomire could have occurred during the late stages of peatification. As mentioned above, the paragenesis of barite monomineralic cleat/fracture infillings (Fig. 10C, D) might not be clear; such monomineralic infillings were presumably formed during either the late stages of peatification and/or epigenetic stages. Previous studies have reported that sulphide and carbonate mono- and polymineralic infillings are mainly related to the precipitation of initial hydrothermal solutions originating from post-Carboniferous dykes and sills in the basin (Karayiğit *et al.*, 2018a, b). The calculated T_{peak} values also imply possible hydrothermal fluids affecting the studied seams; however, the sources of Ca, Mg, Fe, sulphate, and CO_2 seem to be slightly different from those in other parts of the basin since dykes and sills were not observed in the study area, and polymineralic infillings were not common. In the studied samples, monomineralic carbonate and sulphide, and polymineralic carbonate-pyrite cleat/fracture infillings were mostly observed in brecciated vitrinite-bearing samples (Figs. 13C–E; 15D; 16D), which implies that post-coalification tectonic deformation created space for circulating fluids or pore water within coal seams. Thus, fluids leached from overlying Mesozoic marine carbonates via faults precipitated in the cleat/fractures of the studied seams. All these also indicate that the studied Serpukhovian–Bashkirian coals are not as densely affected by heat flow and/or hydrothermal fluids as their counterparts in the northern and central parts of the Zonguldak Basin. Thus, mineral paragenetic sequences in cleat/fractures are slightly different from tectonically affected deeper Serpukhovian–Bashkirian coal seams in the northern and central parts of the Zonguldak Basin.

Hydrocarbon generation potential

During the last two decades, the source rock potential of humic coals has been discussed in detail, and several studies have been conducted on the accuracy of the Rock-Eval pyrolysis analysis of humic coals (*e.g.* Karayigit *et al.*, 2021; Petersen, 2006; Sykes and Snowdon, 2002; Yang and Horsfield, 2020). These studies show that the maceral compositions, thickness of coal seams, H contents, and ranks are key parameters for the hydrocarbon generation potential of humic coal seams. Nevertheless, maceral and mineralogical compositions could affect the programmed pyrolysis process, in turn, misinterpretations of hydrocarbon generation estimations could develop. The ultimate and petrographic analyses suggest that the studied working coal seams might have hydrocarbon generation potential, similar to other coal seams in the Zonguldak Basin (*e.g.* Kara-Gülbay *et al.*, 2019; Karayigit *et al.*, 1998, 2018a, b; Ünal-Kartal and Karadirek, 2024; Yalçin *et al.*, 2002). As a traditional approach, the samples were plotted on pseudo-van Kreveln and HI-T_{max} diagrams. The plotting data on the pseudo-van Kreveln diagram shows that type-II kerogen (liptinite) is common in the analysed samples; however, this data is not in agreement with maceral compositions, which implies the predominance of mixed type III-II (vitrinite-liptinite) kerogen compositions (Fig. 6). This difference could be related to the relatively low OI values of the analysed samples. Nevertheless, the plotting data on the HI-T_{max} diagram is increasingly in agreement with maceral compositions, and the analysed samples are plotted on mixed type III-II (vitrinite-liptinite) kerogen and mixed type II-III (liptinite-vitrinite) kerogen areas (Fig. 6). The plotting data also implies that the analysed samples are oil-prone. The previous studies show that Serpukhovian–Bashkirian and Langsettian coal seams in the Zonguldak Basin are mostly condensate-wet gas windows, while Duckmantian–Asturian coal seams are gas-prone (Kara-Gülbay *et al.*, 2019; Karayiğit *et al.*, 2018b; Ünal-Kartal and Karadirek, 2024; Yalçin *et al.*, 2002). This implies that the samples may be sufficiently mature to produce liquid hydrocarbons. Since the HI values are higher than 200mg HC/g TOC, the analysed samples could be oil-prone.

It is well known that the HI values for humic coals could be problematic for source rock assessments due to the presence of H-rich huminite/vitrinite macerals and/or mineral matter (*e.g.* clay minerals) (Petersen, 2006; Sykes and Snowdon, 2002; Yang and Horsfield, 2020). Considering that the analysed samples are of bituminous rank, the influence of H-rich huminite macerals is not possible. Clay minerals are, on the other hand, the predominant mineral matter in the analysed coals, and S_2 peak measurements might be affected by the breakdown of the OH group in clay minerals during pyrolysis. Additionally, in some cases, the high total S contents and pyrite could also affect the S_2 peak measurements (Petersen, 2006). Therefore, Rock-Eval pyrolysis parameters, particularly the HI values, should be evaluated with caution. Considering the presence of –OH groups in the FT-IR spectra of analysed samples and high S contents of the sample, HI values of the samples might be affected by –OH groups in clay minerals and pyrite grains in the samples. Contrary, the total S contents and clay mineral contents on a whole-coal basis do not display any meaningful correlations with S_2, T_{max}, and HI values, which implies that relatively high HI values are not related to the impact of mineral matter on the pyrolysis process. Furthermore, breakdown of H-rich organic compounds (*e.g.* carboxyl and hydroxyl) in humic coal could also affect S_2 peak measurements and cause relatively low HI values (Karayigit *et al.*, 2021; Petersen, 2006). The presence of

board bands around 2900cm^{-1} in the FT-IR spectra could be indicator of H-rich compounds in the samples (Chen *et al.*, 2013). Therefore, calculated HI values from Rock-Eval pyrolysis data of the samples should be recalculated. To overcome possible influences on S_2 peak measurements, the effective HI and HI_{max} values of the samples were calculated according to Sykes and Snowdon (2002) and Petersen (2006), respectively (Fig. 18).

The calculated effective HI values using the modified HI-T_{max} diagram values are again higher than 200mg HC/g TOC, and the samples are in the early oil generation zone (Fig. 18A). Similarly, the HI_{max} values are calculated between 235–290mg HC/g TOC, which implies oil generation potential (Fig. 18B). Although the calculated HI_{max} values are higher than 200mg HC/g TOC, none of the samples are located in the early oil generation zone in the %VR-HI diagram. All these imply that the studied samples are the on-set of oil-generation potential; however, liquid hydrocarbon generation seems to be very limited due to the rare existence of exsudatinite maceral and low Oil Saturation Index (OSI) values (3.5–6.0mg HC/g TOC) of the samples. Furthermore, the PI (0.01–0.02), QI (2.2–2.9), and BI (0.03–0.06) values also suggest that the analysed samples are mainly gas-prone (Table 4), like the Duckmantian–Asturian coal seams in the basin (Kara-Gülbay *et al.*, 2019; Karayigit *et al.*, 2018b; Ünal-Kartal and Karadirek, 2024). Considering the predominance of vitrinite group macerals in the studied samples, the existence of disseminated liptinite macerals within the humic matrix of detrovitrinite macerals, increased S_2 and HI values are expectable (Fig. 4A–F). Hence, the analysed samples display high S_2, HI, and T_{max} values, similar to those of oil-prone humic coal.

The analysed Serpukhovian–Bashkirian coals from the Kurtköy coalfield display slightly higher OI (4–6mg CO_2/g TOC) values, and relatively lower TOC (48.0–58.3%) contents and T_{max} values than the Serpukhovian–Bashkirian coal seams cored in the deep research wells in the northern parts of the Zonguldak Basin (Yalçin *et al.*, 2002). The differences in OI values may be related to the mineralogical compositions of the analysed samples from the Kurtköy coalfield. Considering the common presence of cleat/fracture carbonate infillings in the analysed samples, their breakdown during pyrolysis could affect the S_3 peak measurement (Karayigit *et al.*, 2021; Lafargue *et al.*, 1998); in turn, the OI and MINC values of the samples were elevated. This could have also caused relatively lower TOC. The slightly lower T_{max} values are controlled by the relatively lower degree of coalification of the studied coals than those cored in the deep research wells in the northern parts of the Zonguldak Basin. The HI values of the samples are significantly higher than those of Serpukhovian–Bashkirian coal seams from the northern parts of the basin and show similar HI values to those of Langsettian and Duckmantian–Asturian coal seams within the Kozlu and Karadon fms. (Kara-Gülbay *et al.*, 2019; Karayiğit *et al.*, 2018b; Yalçin *et al.*, 2002; Ünal-Kartal and Karadirek, 2024). Since the coalification degree and total liptinite contents of Serpukhovian–Bashkirian coals in the Kurtköy coalfield are close to those of coal seams within the Kozlu and Karadon fms., similar HI values could be expected. The higher HI values of the samples could be related to their relatively lower coalification in comparison with their Serpukhovian–Bashkirian counterparts in the northern parts of the basin, where liptinite contents are very low and were emostly observed as relics (Karayiğit *et al.*, 2018a, b). In contrast, liptinite macerals in the studied samples displayed a relatively higher orange fluorescent colour, and cytoplasm spore-fillings were preserved. Therefore, H-rich lipid compounds presumably still existed in the samples; consequently, the HI values of the studied samples are relatively higher than their counterparts in the northern parts of the basin. Overall, the differences in the Rock-Eval

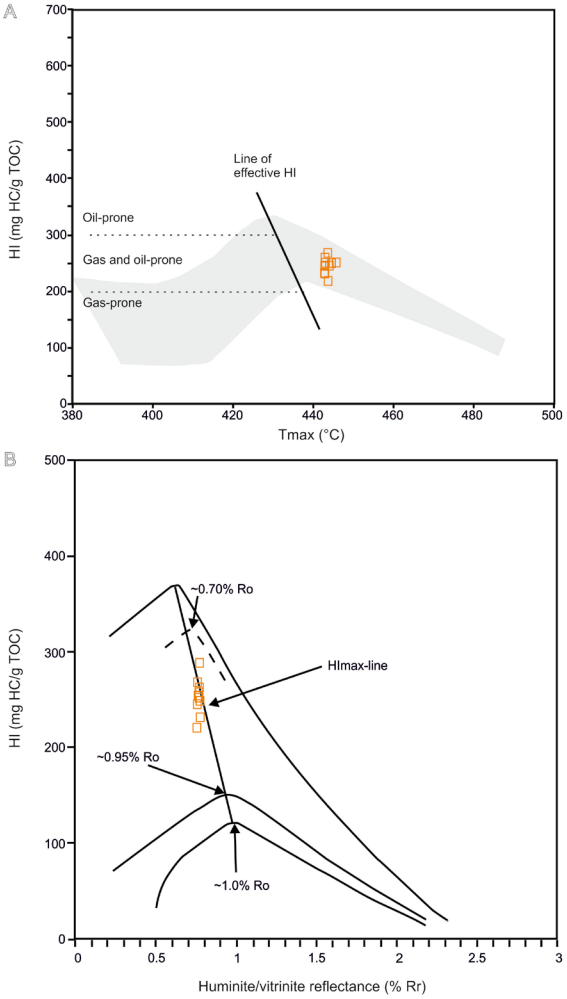

FIGURE 18. Plot of studied samples on modified A) HI-Tmax diagram (after Sykes and Snowdon, 2002) and B) HI-VR diagram (after Petersen, 2006).

pyrolysis data between the studied coal seams and their counterpart Serpukhovian–Bashkirian coal seams in the northern parts of the Zonguldak Basin could be controlled by their degree of coalification.

CONCLUSIONS

The studied Serpukhovian–Bashkirian coals within the Alacaağzı Fm. in the Kurtköy area (SE Zonguldak Basin) display rank differences compared with their counterparts in the northern parts of the basin. The studied working seams are of bituminous C (medium-rank C). Their %Rr (0.76–0.78%±0.02) values are generally lower than other Serpukhovian–Bashkirian coal seams in the northern parts of the basin. The relatively low %Rr values of the studied seams in comparison with other Serpukhovian–Bashkirian coal seams within the Alacaağzı Fm. are presumably related to their relatively lower recent burial depths. This relatively lower rank is also evident with the slightly low T_{peak} (113–127ºC) values and the existence of possibly preserved cytoplasm spore-filling within the macro-sporinites. Hence, this may allow for the preservation of H-rich compounds in the seams. In turn, their HI (221–288mg HC/g rock) values could easily may imply a mixed hydrocarbon generation potential. However, the relatively low OSI values and rare existence of exsudatinite suggest only gas generation potential.

The authigenic syngenetic mineral formation in the studied seams was controlled by redox conditions and epiclastic and/or synchronous volcanic inputs into the palaoemires. Tectonic deformations in the Zonguldak Basin after the Late Carboniferous appear to have caused the formation of brecciated vitrinite grains and created space for the circulation of Ca- and Si-rich pore water and/or hydrothermal fluids within the studied coal seams. Thus, authigenic epigenetic carbonate minerals (*e.g.* calcite and Fe-dolomite/ankerite) and to lesser extent pyrite and kaolinite formation occurred within the cleats/fractures of the studied seams. The cleat/fracture carbonate infillings also caused relatively higher volatile matter contents in the studied seams. Overall, the rank and maturity of the studied seams are controlled by post-coalification regional tectonic movements, while mineralogical compositions seem to be controlled by both depositional conditions within the palaeomires and circulated fluids within the cleat/fracture of the coal seams, which were likely created by tectonic deformation.

ACKNOWLEDGMENTS

This research received no external. The author would like to thank Dr. Vayia Xanathopolou (University of Patras), Mr. Şendoğan Özat (TTK), Mr. Ufuk Kibar (MTA), and Dr. Hüsnü Çorbacı (TPAO), Ms. Başak KARAHAN (Hacettepe University) for their help during different stages of analyses.

REFERENCES

Akgün, F., Akyol, E., 1992. Palynology and paleoecology of the coals in the Amasra-Bartın Carboniferous Basin (In Turkish). Turkish Journal Earth Sciences, 1, 49-56.

Akyol, E., 1974. Etudes palynologiques des veines du Namurien et du Westphalien A, recoupees par les ailes sud et est d'une galerie de cote —50 a Asma, Üzülmez-Zonguldak (In French). Bulletin of the Mineral Research and Exploration, 82, 1-20.

American Society for Testing and Materials (ASTM) D2797/D2797M, 2021. Standard practice for preparing coal samples for microscopical analysis by reflected light. West Conshohocken, ASTM International, 5 pp.

American Society for Testing and Materials (ASTM) D3174, 2018. Standard test method for ash in the analysis sample of coal and coke from coal. West Conshohocken, ASTM International, 6 pp.

American Society for Testing and Materials (ASTM) D3175, 2020. Standard test method for volatile matter in the analysis sample of coal and coke. West Conshohocken, ASTM International, 14 pp.

American Society for Testing and Materials (ASTM) D3302, 2023. Standard test method for total moisture in coal. West Conshohocken, ASTM International, 10 pp.

American Society for Testing and Materials (ASTM) D388, 2018. Standard classification of coals by rank. West Conshohocken, ASTM International, 7 pp.

American Society for Testing and Materials (ASTM) D4239, 2018. Standard test method for sulfur in the analysis sample of coal and coke using high-temperature tube furnace combustion. West Conshohocken, ASTM International, 8 pp.

American Society for Testing and Materials (ASTM) D5373, 2021. Standard test methods for determination of carbon, hydrogen and nitrogen in analysis samples of coal and carbon in analysis samples of coal and coke. West Conshohocken, ASTM International, 11 pp.

American Society for Testing and Materials (ASTM) D5865, 2019. Standard test method for gross calorific value of coal and coke. West Conshohocken, ASTM International, 19 pp.

Arostegui, J., Arroyo, X., Nieto, F., Bauluz, B., 2019. Evolution of clays in Cretaceous Marly series (Álava block, Basque Cantabrian Basin, Spain): Diagenesis and detrital input control. Minerals, 9, 40. DOI: 10.3390/min9010040

Ağralı, B. 1970. Étude des microspores du bassin Carbonifère d'Amasra. Bulletin of the Mineral Research and Exploration, 75, 28-68.

Bansal, O.P., 1983. Thermodynamics of exchange in clays: Ion exchange equilibria of transition metals and sodium ions on illite. Proceedings of the Indian Academy of Sciences

- Chemical Sciences, 92, 589-596. DOI: https://doi.org/10.1016/0022-1902(81)80403-4

Barker, C.E., Pawlewicz, M.J., 1994. Calculation of vitrinite reflectance from thermal histories and peak temperatures. In: Mukhopadhyay, P.K., Dow, W.G. (eds.). Vitrinite Reflectance as a Maturity Parameter. Washington, DCACS Symposium Series, 570, 216-229.

Beyssac, O., Goffé, B., Chopin, C., Rouzaud, J.N., 2002. Raman spectra of carbonaceous material in metasediments: a new geothermometer. Journal of Metamorphic Geology, 20, 859-871. DOI: https://doi.org/10.1046/j.1525-1314.2002.00408.x

Bohor, B.F., Triplehorn, D.M., 1993. Tonsteins: Altered volcanic-ash layers in coal-bearing sequences. Geological Society of America Special Paper 285, Boulder, Geological Society of America, 44 pp.

Bozkaya, Ö., Günal-Türkmenoğlu, A., Göncüoğlu, M.C., Ünlüce, Ö., Yilmaz, İ.Ö., Schroeder, P.A., 2016. Illitization of Late Devonian-Early Carboniferous K-bentonites from Western Pontides, NW Turkey: Implications for their origin and age. Applied Clay Science, 134, 257-274.

Burger, K., Bandelow, F.K., Bieg, G., 2000. Pyroclastic kaolin coal – tonsteins of the Upper Carboniferous of Upper Carboniferous of Zonguldak and Amasra, Turkey. International Journal of Coal Geology, 45, 39-53.

Cao, Y., Davis, A., Li, R., Liu, X., Zhang, Y., 2003. The influence of tectonic deformation on some geochemical properties of coals-a possible indicator of outburst potential. International Journal of Coal Geology, 53, 69-79.

Chen, Y., Caro, L.D., Mastalerz, M., Schimmelmann, A., Blandón, A., 2013. Mapping the chemistry of resinite, funginite and associated vitrinite in coal with micro-FTIR. Journal of Microscopy, 249, 68-81.

Cleal, C.J., van Waveren, I.M., 2012. A reappraisal of the Carboniferous macrofloras of the Zonguldak – Amasra Coal Basin, north-western Turkey. Geologica Croatica, 65, 283-297.

Dai, S., Bechtel, A., Eble, C.F., Flores, R.M., French, D., Graham, I.T., Hood, M.M., Hower, J.C., Korasidis, V.A., Moore, T.A., Püttmann, W., Wei, Q., Zhao, L., O'Keefe, J.M.K., 2020. Recognition of peat depositional environments in coal: A review. International Journal of Coal Geology, 219, 103383. DOI: https://doi.org/10.1016/j.coal.2019.103383

Dai, S., Hower, J.C., Ward, C.R., Guo, W., Song, H., 2015. Elements and phosphorus minerals in the middle Jurassic inertinite-rich coals of the Muli Coalfield on the Tibetan Plateau. International Journal of Coal Geology, 144-145, 23-47. DOI: https://doi.org/10.1016/j.coal.2015.04.002

Dai, S., Ward, C.R., Graham, I.T., French, D., Hower, J.C., Zhao, L., Wang, H., 2017. Altered volcanic ashes in coal and coal-bearing sequences: A review of their nature and significance. Earth-Science Reviews, 175, 44-74. DOI: https://doi.org/10.1016/j.earscirev.2017.10.005

Dawson, G.K.W., Golding, S.D., Esterle, J.S., Massarotto, P., 2012. Occurrence of minerals within fractures and matrix of selected Bowen and Ruhr Basin coals. International Journal of Coal Geology, 9, 150-166.

Deon, F., van Ruitenbeek, F., van der Werff, H., van der Meijde, M., Marcatelli, C., 2022. Detection of interlayered illite/smectite clay minerals with XRD, SEM analyses and reflectance spectroscopy. Sensors, 22, 9. DOI: https://doi.org/10.3390/s22093602

Economic Commission for Europe-United Nations (E.C.E.-U.N.), 1998. International classification of in-seam coals. Geneva, ECE Energy, 42 pp.

Espitalié, J., Laporte, J., Madec, M., Marquis, F., Leplat, P., Boutefeu, A., 1977. Rapid method for source rock characterization, and for determination of their petroleum potential and degree of evolution. Oil & Gas Science and Technology, 32, 23-42.

Fisne, A., Esen, O., 2014. Coal and gas outburst hazard in Zonguldak Coal Basin of Turkey, and association with geological parameters. Natural Hazards, 74, 1363-1390.

Frodsham, K., Gayer, R.A., 1999. The impact of tectonic deformation upon coal seams in the South Wales coalfield, UK. International Journal of Coal Geology, 38, 297-332.

Furuichi, H., Ujiie, K., Kouketsu, Y., Saito, T., Tsutsumi, A., Wallis, S., 2015. Vitrinite reflectance and Raman spectra of carbonaceous material as indicators of frictional heating on faults: Constraints from friction experiments. Earth and Planetary Science Letters, 424, 191-200.

Georgakopoulos, A., Iordanidis, A., Kapina, V., 2003. Study of low rank Greek coals using FTIR spectroscopy. Energy Sources, 25, 995-1005.

Gorur, N., Tuysuz, O., Aykol, A., Sakinc, M., Yigitbas, E., Akkok, R., 1993. Cretaceous red pelagic carbonates of northern Turkey: their place in the opening history of the Black Sea. Eclogae Geologicae Helvetiae, 86, 819-838.

Guedes, A., Valentim, B., Prieto, A.C., Rodrigues, S., Noronha, F., 2010. Micro-Raman spectroscopy of collotelinite, fusinite and macrinite. International Journal of Coal Geology, 83, 415-422.

Hackley, P.C., Lünsdorf, N.K., 2018. Application of Raman spectroscopy as thermal maturity probe in shale petroleum systems: insights from natural and artificial maturation series. Energy and Fuels, 32, 11190-11202.

Hinrichs, R., Brown, M.T., Vasconcellos, M.A.Z., Abrashev, M.V., Kalkreuth, W., 2014. Simple procedure for an estimation of the coal rank using micro-Raman spectroscopy. International Journal of Coal Geology, 136, 52-58.

Hower, J.C., Eble, C.F., 2022. Petrology, palynology, and geochemistry of the Pond Creek coal (Pennsylvanian, Duckmantian), Pike County, Kentucky: Overprints of penecontemporaneous tectonism and peat doming. International Journal of Coal Geology, 258, 104027. DOI: https://doi.org/10.1016/j.coal.2022.104027

Hower, J.C., Eble, C.F., Mastalerz, M., 2022. Petrology of the Fire Clay coal, Bear Branch, Perry County, Kentucky. International Journal of Coal Geology, 249, 103891. DOI: https://doi.org/10.1016/j.coal.2021.103891

Hower, J.C., Rimmer, S.M., Mastalerz, M., Wagner, N.J., 2021. Migmatite-like textures in anthracite: Further evidence for low-grade metamorphic melting and resolidification in high-

rank coals. Geoscience Frontiers, 12, 101122. DOI: https://doi.org/10.1016/j.gsf.2020.12.004

Hower, J.C., Williams, D.A., Eble, C.F., Sakulpitakphon, T., Moecher, D.P., 2001. Brecciated and mineralized coals in Union County Western Kentucky coal field. International Journal of Coal Geology, 47, 223-234. DOI: https://doi.org/10.1016/S0166-5162(01)00047-7

Hoşgörmez, H., Yalçin, M.N., Cramer, B., Gerling, P., Faber, E., Schaefer, R.G., Mann, U., 2002. Isotopic and molecular composition of coal-bed gas in the Amasra region (Zonguldak Basin-Western Black Sea). Organic Geochemistry, 33, 1429-1439.

International Committee for Coal and Organic Petrology (ICCP), 1998. The new vitrinite Classification. Fuel, 77, 349-358.

International Committee for Coal and Organic Petrology (ICCP), 2001. New inertinite classification (ICCP System 1994). Fuel, 80, 459-471. DOI: https://doi.org/10.1016/S0016-2361(00)00102-2

International Committee for Coal Petrology (ICCP), 1993. International Handbook of Coal Petrography (2nd ed.). 3rd supplement. Paris, Centre National de la Recherche Scientifique, 146 pp.

International Organization for Standardization (ISO) 7404–5, 2009. Methods for the petrographic analysis of coal—part 5: methods of determining microscopically the reflectance of vitrinite. Geneva, ISO, 14 pp.

International Organization for Standardization ISO 11760, 2018. Classification of coals. Geneva, ISO, 9 pp.

Jiang, J., Zhang, S., Longhurst, P., Yang, W., Zheng, S., 2021. Molecular structure characterization of bituminous coal in Northern China via XRD, Raman and FTIR spectroscopy. Spectrochimica Acta, Part A: Molecular and Biomolecular Spectroscopy, 255, 119724. DOI: https://doi.org/10.1016/j.saa.2021.119724

Kara-Gülbay, R., Yaylall-Abanuz, G., Korkmaz, S., Erdoğan, M.S., Hoş-Çebi, F., Çevik, S., Ağlrman-Aktürk, E., 2019. Organic matter type, maturity, depositional environmental characteristics, and liquid hydrocarbon potential of Late Carboniferous Kozlu bituminous coal and coaly shale beds (Zonguldak-Amasra Basin, NW Anatolia, Turkey): An application of biomarker geochemistry. Energy and Fuels, 33, 9491-9509.

Karayigit, A.I., Oskay, R.G., Çelik, Y., 2021. Mineralogy, petrography, and Rock-Eval pyrolysis of late Oligocene coal seams in the Malkara coal field from the Thrace Basin (NW Turkey). International Journal of Coal Geology, 244, 103814. DOI: https://doi.org/10.1016/j.coal.2021.103814

Karayiğit, A.İ., 1991. Investigation of the variations of clay minerals and the illite crystallinite index of Kozlu and Karadon Formations in Zonguldak and Amasra Basin. Journal of Isparta Engineering Faculty of Akdeniz University, Geological Engineering Section, 5, 133-147.

Karayiğit, A.İ., 1992. Linear relations among vitrinite reflections of coals in Zonguldak and Amasra basin (in Turkish). Turkish Journal of Earth Sciences, 1, 43-48.

Karayiğit, A.İ., 2001. Mineralogy and trace element contents of the Akalin seam, Gelik mine, Zonguldak-Turkey. Energy Sources, 23, 699-709.

Karayiğit, A.İ., 2003. Mineralogy and trace element contents of the Upper Carboniferous coals from the Asma-Dilaver and Gelik Mines in Zonguldak, Turkey. Energy Sources, 25, 689-702. DOI: 10.1080/00908310390212417

Karayiğit, A.İ., Cicioğlu Sütcü, E., Temel, A., Gündoğdu, M.N., 2022. Vertical variations of minerals in clayey sedimentary rocks in the cores of two-deep exploration wells from the Kozlu coalfield (Zonguldak, NW Türkiye), with emphasis on tonstein (schieferton) formation. Turkish Journal of Earth Sciences, 31, 97-621.

Karayiğit, A.İ., Gayer, R.A., Demirel, I.H., 1998. Coal rank and petrography of Upper Carboniferous seams in the Amasra Coalfield, Turkey. International Journal of Coal Geology, 36, 277-294. DOI: https://doi.org/10.1016/S0166-5162(97)00047-5

Karayiğit, A.İ., Mastalerz, M., Oskay, R.G., Buzkan, İ., 2018b. Bituminous coal seams from underground mines in the Zonguldak Basin (NW Turkey): insights from mineralogy, coal petrography, Rock-Eval pyrolysis, and meso-and microporosity. International Journal of Coal Geology, 199, 91-112. DOI: https://doi.org/10.1016/j.coal.2018.09.020

Karayiğit, A.İ., Mastalerz, M., Oskay, R.G., Gayer, R.A., 2018a. Coal petrography, mineralogy, elemental compositions and palaeoenvironmental interpretation of Late Carboniferous coal seams in three wells from the Kozlu coalfield (Zonguldak Basin, NW Turkey). International Journal of Coal Geology, 187, 54-70. DOI: https://doi.org/10.1016/j.coal.2017.12.007

Kerey, I.E., 1984. Facies and tectonic setting of the Upper Carboniferous rocks of northwestern Turkey. Geological Society Special Publication, 17, 123-128.

Kerey, I.E., Kelling, G., Wagner, R.H., 1986. An outline stratigraphy and palaeobotanical records from the middle Carboniferous rocks of northwestern Turkey. Annales de la Société Géologique du Nord, 105, 203-216.

Kouketsu, Y., Mizukami, T., Mori, H., Endo, S., Aoya, M., Hara, H., Nakamura, D., Wallis, S., 2014. A new approach to develop the Raman carbonaceous material geothermometer for low-grade metamorphism using peak width. Island Arc, 23, 33-50.

Kruszewska, K.J., Du Cann, V.M., 1996. Detection of the incipient oxidation of coal by petrographic techniques. Fuel, 75, 769-774.

Kus, J., Misz-Kennan, M., 2017. Coal weathering and laboratory (artificial) coal oxidation. International Journal of Coal Geology, 171, 12-36.

Lafargue, E., Marquis, F., Pillot, D., 1998. Rock-Eval 6 Applications in hydrocarbon exploration, production, and soil contamination studies. Oil & Gas Science and Technology, 53, 421-437.

Larsen, D., Mann, R., 2005. Origin of high manganese concentrations in coal mine drainage, eastern Tennessee. Journal of Geochemical Exploration, 86, 143-163.

Li, K., Rimmer, S.M., Liu, Q., Zhang, Y., 2019. Micro-Raman spectroscopy of microscopically distinguishable components

of naturally graphitized coals from Central Hunan Province, China. Energy and Fuels, 33, 1037-1048.

Li, K., Rimmer, S.M., Presswood, S.M., Liu, Q., 2020. Raman spectroscopy of intruded coals from the Illinois Basin: Correlation with rank and estimated alteration temperature. International Journal of Coal Geology, 219, 103369. DOI: https://doi.org/10.1016/j.coal.2019.103369

Li, M., Jiang, B., Lin, S., Wang, J., Ji, M., Qu, Z., 2011. Tectonically deformed coal types and pore structures in Puhe and Shanchahe coal mines in western Guizhou. Mining Science and Technology, 21, 353-357. DOI: https://doi.org/10.1016/j.mstc.2011.05.002

Li, W., Guo, J., Jiao, Y., Deng, D., Zhong, Y., Yang, S., 2023. Investigation on tectonically deformed coal particle crushing by DEM under triaxial loading: Implication for coal and gas outburst. Advanced Powder Technology, 34, 104155. DOI: https://doi.org/10.1016/j.apt.2023.104155

Liu, H., Jiang, B., 2019. Geochemical alteration and mineralogy of coals under the influence of fault motion: a case study of Qi'nan colliery, China. Minerals, 9, 389. DOI: https://doi.org/10.3390/min9070389

Lo, H.B., 1993. Correction criteria for the suppression of vitrinite reflectance in hydrogen-rich kerogens: preliminary guidelines. Organic Geochemistry, 20, 653-657. DOI: https://doi.org/10.1016/0146-6380(93)90051-C

Madejová, J., 2003. FTIR techniques in clay mineral studies. Vibrational Spectroscopy, 31, 1-10. DOI: https://doi.org/10.1016/S0924-2031(02)00065-6

Mangena, S.J., du Cann, V.M., 2007. Binderless briquetting of some selected South African prime coking, blend coking and weathered bituminous coals and the effect of coal properties on binderless briquetting. International Journal of Coal Geology, 71, 303-312. DOI: https://doi.org/10.1016/j.coal.2006.11.001

Mathews, W.H., Bustin, R.M., 1984. Changes associated with natural in situ weathering of a coking coal from southeastern British Columbia. Fuel, 63, 548-550.

Matlala, I.V., Moroeng, O.M., Kalaitzidis, S., Wagner, N.J., 2024. Raman Spectroscopy for the characterization of the macromolecular structure of Highveld coals (South Africa). International Journal of Coal Geology, 288, 104531. DOI: https://doi.org/10.1016/j.coal.2024.104531

Naik, A.S., Behera, B., Shukla, U.K., Sahu, H.B., Singh, P.K., Mohanty, D., Sahoo, K., Chatterjee, D., 2021. Mineralogical Studies of Mahanadi Basin coals based on FTIR, XRD and Microscopy: A Geological Perspective. Journal of the Geological Society of India, 97, 1019-1027.

Okan, Y., Hoşgör, İ., 2007. Late Visean-Early Namurian bivalves from the Zonguldak coal basin, Northwestern Turkey. Turkish Journal of Earth Sciences, 16, 225-240.

Okay, A.I., Nikishin, A.M., 2015. Tectonic evolution of the southern margin of Laurasia in the Black Sea region. International Geology Review, 57, 1051-1076.

Okay, A.İ., Sengor, A.M.C., Gorur, N., 1994. Kinematic history of the opening of the Black Sea and its effect on the surrounding regions. Geology, 22, 267-270.

Okay, A.İ., Tüysüz, O., 1999. Tethyan sutures of northern Turkey. Geological Society Special Publications, 156, 475-515.

Olgun, E., Fisne, A., 2014. Coal and gas outburst hazard in Zonguldak Coal Basin of Turkey, and association with geological parameters. Natural Hazards, 74, 1363-1390.

Opluštil, S., Lojka, R., Pšenička, J., Yilmaz, Ç., Yilmaz, M., 2018. Sedimentology and stratigraphy of the Amasra coalfield (Pennsylvanian), NW Turkey – new insight from a 1 km thick section. International Journal of Coal Geology, 195, 317-346.

Oskay, R.G., Christanis, K., Inaner, H., Salman, M., Taka, M., 2016. Palaeoenvironmental reconstruction of the eastern part of the Karapınar-Ayrancı coal deposit (Central Turkey). International Journal of Coal Geology, 163, 100-111.

O'Keefe, J.M.K., Bechtel, A., Christanis, K., Dai, S., DiMichele, W.A., Eble, C.F., Esterle, J.S., Mastalerz, M., Raymond, A.L., Valentim, B.V., Wagner, N.J., Ward, C.R., Hower, J.C., 2013. On the fundamental difference between coal rank and coal type. International Journal of Coal Geology, 118, 58-87.

Passey, S.R., 2014. The habit and origin of siderite spherules in the Eocene coal-bearing Prestfjall formation, Faroe Islands. International Journal of Coal Geology, 122, 76-90.

Permana, A.K., Ward, C.R., Li, Z., Gurba, L.W., 2013. Distribution and origin of minerals in high-rank coals of the South Walker Creek area, Bowen Basin, Australia. International Journal of Coal Geology, 116-117, 185-207.

Peters, K.E., 1986. Guidelines for evaluating petroleum source rock using programmed pyrolysis. APPG Bulletin, 70, 318-329.

Petersen, H.I., 2006. The petroleum generation potential and effective oil window of humic coals related to coal composition and age. International Journal of Coal Geology, 67, 221-248. DOI: https://doi.org/10.1016/j.coal.2006.01.005

Pickel, W., Kus, J., Flores, D., Kalaitzidis, S., Christanis, K., Cardott, B.J., Misz-Kennan, M., Rodrigues, S., Hentschel, A., Hamor-Vido, M., Crosdale, P., Wagner, N., ICCP 2017. Classification of liptinite – ICCP System 1994. International Journal of Coal Geology, 169, 40-61. DOI: https://doi.org/10.1016/j.coal.2016.11.004

Rao, P.D., Walsh, D.E., 1997. Nature and distribution of phosphorus minerals in Cook Inlet coals, Alaska. International Journal of Coal Geology, 33, 19-42. DOI: https://doi.org/10.1016/0166-5162(95)00045-3

Rao, P.D., Walsh, D.E., 1999. Influence of environments of coal deposition on phosphorous accumulation in a high latitude, northern Alaska, coal seam. International Journal of Coal Geology, 38, 261-284. DOI: https://doi.org/10.1016/S0166-5162(98)00026-3

Ren, J., Weng, H., Li, B., Chen, F., Liu, J., Song, Z., 2022. The influence mechanism of pore structure of tectonically deformed coal on the adsorption and desorption hysteresis. Frontiers in Earth Science, 10, 1-16.

Schito, A., Romano, C., Corrado, S., Grigo, D., Poe, B., 2017. Diagenetic thermal evolution of organic matter by Raman spectroscopy. Organic Geochemistry, 106, 57-67.

Scott, A.C., Glasspool, I.J., 2007. Observations and experiments on the origin and formation of inertinite group macerals. International Journal of Coal Geology, 70, 53-66.

Shen, M., Dai, S., French, D., Graham, I.T., Spiro, B.F., Wang, N., Tian, X., 2023. Geochemical and mineralogical evidence for the formation of siderite in Late Permian coal-bearing strata from western Guizhou, SW China. Chemical Geology, 637, 121675.

Siavalas, G., Linou, M., Chatziapostolou, A., Kalaitzidis, S., Papaefthymiou, H., Christanis, K., 2009. Palaeoenvironment of Seam I in the Marathousa Lignite Mine, Megalopolis Basin (Southern Greece). International Journal of Coal Geology, 78, 233-248.

Spears, D.A., 2012. The origin of tonsteins, an overview, and links with seatearths, fireclays and fragmental clay rocks. International Journal of Coal Geology, 94, 22-31.

Stout, S.A., Spackman, W., 1987. A microscopic investigation of woody tissues in peats: some processes active in the peatification of lignocellulosic cell walls. International Journal of Coal Geology, 8, 55-68.

Sykes, R., Snowdon, L.R., 2002. Guidelines for assessing the petroleum potential of coaly source rocks using Rock-Eval pyrolysis. Organic Geochemistry, 33, 1441-1455.

Tironi, A., Trezza, M.A., Irassar, E.F., Scian, A.N., 2012. Thermal treatment of kaolin: effect on the pozzolanic activity. Applied Clay Science, 20, 343-350.

Tüysüz, O., 1999. Geology of the Cretaceous sedimentary basins of the Western Pontides. Geological Journal, 34, 75-93.

Tüysüz, O., 2018. Cretaceous geological evolution of the Pontides. Geological Society Special Publication, 464, 69-94.

Tüysüz, O., Melinte-Dobrinescu, M.C., Yılmaz, İ.Ö., Kirici, S., Švabenická, L., Skupien, P., 2016. The Kapanboğazı formation: A key unit for understanding Late Cretaceous evolution of the Pontides, N Turkey. Palaeogeography, Palaeoclimatology, Palaeoecology, 441, 565-581.

Uguna, J.O., Carr, A.D., Marshall, C., Large, D.J., Meredith, W., Jochmann, M., Snape, C.E., Vane, C.H., Jensen, M.A., Olaussen, S., 2017. Improving spatial predictability of petroleum resources within the Central Tertiary Basin, Spitsbergen: A geochemical and petrographic study of coals from the eastern and western coalfields. International Journal of Coal Geology, 179, 278-294.

Valentim, B., Algarra, M., Guedes, A., Rodriguez-Borges, J.E., Da Silva, J.C.G., Suárez-Ruiz, I., 2013. Coal rank increase and aerial oxidation by a combination of Fourier transform infrared spectroscopy with multivariate analysis. Spectroscopy Letters, 46, 277-285.

van Groeningen, N., Glück, B., Christl, I., Kretzschmar, R., 2020. Surface precipitation of Mn^{2+} on clay minerals enhances Cd^{2+} sorption under anoxic conditions. Environmental Science: Processes & Impacts, 22, 1654-1665.

Vu, T.T.A., Horsfield, B., Mahlstedt, N., Schenk, H.J., Kelemen, S.R., Walters, C.C., Kwiatek, P.J., Sykes, R., 2013. The structural evolution of organic matter during maturation of coals and its impact on petroleum potential and feedstock for the deep biosphere. Organic Geochemistry, 62, 17-27.

Wang, H., Shi, X., Tian, J., Pan, J., Yao, L., Feng, X., 2021. Macromolecular structure changes of tectonically deformed coal: evidence from coal pyrolysis, 13C NMR, and XRD experiments. Energy and Fuels, 35, 8711-8722.

Wang, J., Evangelou, V.P., Creech, B., 1993. Characteristics of manganese-calcium exchange behavior on kaolinite and illite and pH influence. Journal of Environmental Science and Health. Part A: Environmental Science and Engineering and Toxicology, 28, 1381-1391. DOI: https://doi.org/10.1080/10934529309375948

Ward, C.R., 2002. Analysis and significance of mineral matter in coal seams. International Journal of Coal Geology, 50, 135-168. DOI: https://doi.org/10.1016/S0166-5162(02)00117-9

Ward, C.R., 2016. Analysis, origin and significance of mineral matter in coal: an updated review. International Journal of Coal Geology, 165, 1-27. DOI: https://doi.org/10.1016/j.coal.2016.07.014

Xie, P., Hower, J.C., Liu, X., 2019. Petrographic characteristics of the brecciated coals from Panxian County, Guizhou, southwestern China. Fuel, 243, 1-9. DOI: https://doi.org/10.1016/j.fuel.2019.01.096

Yalçin, M.N, Seyis, C., Inan, S., 2023. Rank of Kozlu Formation coals in the Zonguldak Basin: implications for coalbed gas. Turkish Journal of Earth Sciences, 32, 808-818. DOI: 10.55730/1300-0985.1875

Yalçin, M.N., Inan, S., Gürdal, G., Mann, U., Schaefer, R.G., 2002. Carboniferous coals of the Zonguldak basin (northwest Turkey): implications for coalbed methane potential. APPG Bulletin, 86, 1305-1328.

Yang, S., Horsfield, B., 2020. Critical review of the uncertainty of Tmax in revealing the thermal maturity of organic matter in sedimentary rocks. International Journal of Coal Geology, 225, 103500. DOI: https://doi.org/10.1016/j.coal.2020.103500

Yilmaz, Y., Tüysüz, O., Yigitbaş, E., Genç, Ş.C., Şengör, A.M.C., 1997. Geology and tectonic evolution of the Pontides. In: Robinson, A.G. (ed.). Regional and petroleum geology of the Black Sea and surrounding region. AAPG Memoir, 68, 183-226.

Zhao, L., Ward, C.R., French, D., Graham, I.T., 2012. Mineralogy of the volcanic-influenced Great Northern coal seam in the Sydney Basin, Australia. International Journal of Coal Geology, 94, 94-110. DOI: https://doi.org/10.1016/j.coal.2011.09.010

Zhao, L., Ward, C.R., French, D., Graham, I.T., Dai, S., Yang, C., Xie, P., Zhang, S., 2018. Origin of a kaolinite-NH_4-illite-pyrophyllite-chlorite assemblage in a marine-influenced anthracite and associated strata from the Jincheng Coalfield, Qinshui Basin, Northern China. International Journal of Coal Geology, 185, 61-78. DOI: https://doi.org/10.1016/j.coal.2017.11.013

Zhou, M., Dai, S., Wang, X., Zhao, L., Nechaev, V.P., French, D., Graham, I.T., Zheng, J., Wang, Y., Dong, M., 2022. Critical element (Nb-Ta-Zr-Hf-REE-Ga-Th-U) mineralization in Late Triassic coals from the Gaosheng Mine, Sichuan Basin, southwestern China: Coupled effects of products of sediment-source-region erosion and acidic water infiltration.

International Journal of Coal Geology, 262, 104101. DOI: https://doi.org/10.1016/j.coal.2022.104101

Zijlstra, G., 1952. Erosion of the Namurian during the Westphalian b-c in the Zonguldak coal field (Turkey). Bulletin of the Mineral Research and Exploration, 42-43, 121-122.

Çelik, Y., Karayigit, A.I., Oskay, R.G., Kayseri-Özer, M.S., Christanis, K., Hower, J.C., Querol, X., 2021. A multidisciplinary study and palaeoenvironmental interpretation of middle Miocene Keles lignite (Harmancık Basin, NW Turkey), with emphasis on syngenetic zeolite formation. International Journal of Coal Geology, 237, 103691. DOI: https://doi.org/10.1016/j.coal.2021.103691

Çetinkaya, S., Yürüm, Y., 2000. Oxidative pyrolysis of Turkish lignites in air up to 500°C. Fuel Processing Technology, 67, 177-189.

Ünal-Kartal, N., Karadirek, S., 2024. Paleoenvironmental reconstruction and hydrocarbon potential of the Westphalian-A Kozlu Formation hard coal in the Zonguldak Basin: Insights from organic geochemistry and petrology. Minerals, 14, 971.

Manuscript received March 2025;
revision accepted May 2025;
published Online July 2025.